Report for the Third of Three Years
for Grant NAGW-3417
from the NASA Planetary Atmospheres Program

STUDIES OF TENUOUS PLANETARY ATMOSPHERES

Research Area: Composition/Structure/Dynamics of Comet and Planetary Satellite Atmospheres

Original Starting Date: January 1, 1993
End Date: December 31, 1995

Principal Investigator: Dr. Michael R. Combi

Space Physics Research Laboratory
Department of Atmospheric, Oceanic and Space Sciences
The University of Michigan
Ann Arbor, Michigan
(313) 764-7226

ANNUAL REPORT

I. Project Overview

Scientific Objectives A 3-year program of research is described that addresses two cases of tenuous planetary atmospheres: comets and Io. Funding for a continuation of this project for another year has already been tentatively approved.

Comets In order to understand the physical and chemical processes that produce the observed spatial morphology of the cometary coma, it is necessary to analyze observational data with physically meaningful models. With this in mind, the goals of this project are to complement our program of theoretical modeling with observational data analysis regarding the spatial distributions of neutral gases and dust in the coma. More specifically the proposed comet atmosphere research focusses on three problems.

• *To analyze a set of spatial profiles of CN in comet Halley taken by three observers that cover a complete 7.4-day period in April 1986. The object is to specify the time synchronization of the parent molecule production at the nucleus (and not just the response of the daughters), and to separate the effects of photochemical lifetimes and velocities.*

• *To apply our newly -developed dust coma model to various observations. The model is a fully 3-D time-dependent treatment of dust particle trajectories which is based on the foundation of our H coma model. Realistic physics of light scattering by dust, dust radiation-pressure efficiencies, and dust terminal ejection velocities are included. We will address such issues as day/night dust production, dust particle size distributions and dust fragmentation-vaporization.*

• *To analyze observations of the inner hydrogen coma, which can be optically thick to the resonance scattering of Lyman-α radiation, with the newly developed approach that combines a spherical radiative transfer model with our Monte Carlo H coma model. Data will include published wide field rocket and spacecraft data.*

Io The production of atmospheric gases from Io's volcanoes, the condensation, and sublimation of the resulting surface frosts, and the combination of direct (ionization, charge impact and charge exchange) and indirect (atmospheric heating and atmospheric sputtering) magnetospheric wind-driven processes are important both for shaping the structure of Io's local atmosphere and for establishing the conditions for escape of that atmosphere and the ultimate injection of heavy ions into Jupiter's plasma torus. In order to establish a theoretical basis for a variety of related problems associated with Io's atmosphere and its interaction with the plasma torus we propose to apply basic methods and years of experience in treating a variety of gasdynamic problems for comets and extended atmosphere studies on Io, and specifically

• *To study the atmospheric escape from Io with a hybrid-kinetic model for neutral gases and plasma given methods and algorithms developed for the study of neutral gas cometary atmospheres and the earth's polar wind and plasmasphere.*

II. Progress Report

The principal parts of the comet portion of the work have gone through the complete cycle of planning, work, and publication. One publication in each of the three areas of comet study has been published during the second and third years of the project. In these areas the work involved application and modification of models which have been developed over more than a decade in some cases. For each of these papers, all of the PI's contribution is credited to this project alone. The Io portion of the work, on the other hand, represents a major new modeling effort. In the fourth part of section II.B. we present preliminary results from the Io model, giving the first 2-D axisymmetric kinetic atmosphere model. We plan one publication on first results before the end of the current project year, and substantial progress toward a major paper on a full model including photochemistry, radiational cooling and a complete set of neutral and ion species.

Cometary Hydrogen Lyman-α Studies We have applied the coupled radiative transfer/Monte Carlo H coma model to the Pioneer Venus Lyman-α observations of comet Halley, as part of a collaboration with W.H. Smyth and M.L Marconi (AER, Inc.) in order to verify the approximate radiative transfer used in the usual analysis of those wide field scans. As part of this collaboration, a paper has been written and published describing the analysis of the spatial profiles contained in that data set (Smyth, Marconi, & Combi 1995). The major results are that the hydrogen Monte Carlo particle trajectory model (MCPTM), developed several years ago (Combi & Smyth 1988 a&b), can reproduce the spatial profiles observed by the PVOUVS (Pioneer Venus Orbiter Ultraviolet Spectrometer) covering a period from late December, 1985 (r~1AU preperihelion), to the time of the spacecraft flybys in early March, 1986 (r~0.85 AU postperihelion). Water production rates calculated from the data using the model brings the PVOUVS and IUE water production into much better agreement. Furthermore, the results imply that the largest water production rates for Halley likely occurred during late January, 1986, one to two weeks before perihelion. A reprint of this paper is attached to the Appendix of this report.

Time-Series Analysis of Cometary Spatial Profiles In the early comprehensive studies of spatial profiles of molecular species in comets, Combi & Delsemme (1980b & 1986) warned of the influence of the irregular time-variation of the parent gas production rate on the shapes of the profiles. Their conclusion was that, provided many spatial profiles taken at different times are analyzed, fitted scale lengths (using Haser's model) or lifetimes (using vectorial or Monte Carlo models) could be determined in a statistical manner, and the effect of gas production rate could be

in a sense be averaged out. This was borne out by the results of Fink, Combi & DiSanti (1991) whose Haser model analyses of observations of spatial profiles in comet Halley were generally consistent on the average with those of other comets, despite the now well-known large amplitude periodic variation in the post-perihelion period.

Combi & Fink (1993) presented a time-dependent model analysis of two sets of pairs of spatial profiles of each of C_2, CN, NH_2 and $O(^1D)$, obtained on March 1 and 2, and April 14 and 15, 1986. We used the photometry of Schleicher et al. (1990a) as a basis for the time varying production rate but allowed for an adjustable phase shift and amplitude enhancement between the source at the nucleus and the response of the coma at seen in the photometric aperture. We found that spatial profiles, which varied significantly from March 1 to March 2 and from April 14 to April 15, could be consistently modeled for all four species accounting for time dependence with only "average" scale lengths. We were then able to assemble a set spatial profiles of CN constructed from observations taken by Dr. Anita Cochran of the University of Texas, and Dr. Rita Schulz of the University of Maryland during the same time period which taken together with the first observations provide a time-series of CN spatial profiles spanning just over one 7.4-day period from April 7 to April 15, 1986. Schulz's observations were particularly interesting because of the very large spatial scale covered which allows tracking of the gas production waves (or haloes in 2-D) out to 10^6 km.

This time sequence of 8-days of CN spatial profiles has been analyzed using the time-dependent Monte Carlo model, and can be explained with the same model parameters (scale lengths, and phase-lag and amplitude compression of the light curve) as had been used previously for only the April 14 and 15 profiles. The most interesting aspect of these results is that the wavy features predicted to occur at large distances from the nucleus in the previous paper (that was based only on data from within 10^5 km from the nucleus), were in fact found in the extended spatial profiles from the observations of R. Schulz. A paper describing these results was written, submitted and published in the Astrophysical Journal (Combi et al. 1994). A reprint of this paper is attached to the Appendix of this report.

Model Analysis of the Dust Comae of Comets The newly developed dust model was applied to study the effect of fragmentation of dust particles on the shapes of isophotes in the dust coma. Dust particles when released from the nucleus of a comet are entrained in the expanding gas flow created by the vaporization of ices (mainly water ice). Traditional approaches to dusty-gas dynamics in the inner comae of comets consider there to be an initial distribution of dust particle sizes which do not fragment or evaporate. Dusty-gas dynamics based on the Finson-Probstein (1968 a&b) model yields a 1-to-1-to-1 correspondence between the size of a dust particle, its

terminal velocity owing to gas drag, and its radiation pressure acceleration which creates the notable cometary dust tail.

Using the experience gained in dealing with modeling the H coma (Combi & Smyth 1988b) and the newly developed dust coma model, it was clear that the typical elongated shapes of the antisunward isophotes in the dust comae of comets on the scale of $> 10^4$ km from the nucleus requires that the one-to-one-to-one relationship cannot in general be correct. There must be a broad range of velocities for any particle size, including small particles having a small velocity but large radiation pressure acceleration, in order to explain the elongated shape. A way to create such a distribution is if particle fragmentation, or some combination of fragmentation with vaporization, routinely occurs within and/or just outside of the dusty-gas acceleration region (i.e. up to several hundred km). In this way initially large particles, which are accelerated to fairly slow velocities by gas-drag, fragment to form small particles which still move slowly but are subject to a relatively large radiation pressure acceleration. Fragmentation has already been suggested as one possible interpretation for the flattened gradient in the spatial profiles of dust extracted from Giotto images of Comet Halley. Grain vaporization has been suggested as a possible spatially extended source of coma gases. The general elongated isophote shapes seen in ground-based images for many years represents another possible signature of fragmentation. The results were presented at the 1993 DPS meeting and published in The Astronomical Journal (Combi 1994). A reprint of this paper is attached to the Appendix of this report.

A Global Kinetic Atmosphere Model of Io The other main topic in tenuous atmosphere modeling is to study the global structure of Io's atmosphere its interaction with the Jupiter/Io plasma torus, and the large escape rate of neutral gases. The first method we considered for doing this was to apply a 2-D axisymmetric adaptive mesh code, which has been acquired from the U. of Michigan Aerospace Engineering group in order to construct a lower atmosphere model for Io. This is a more advanced and numerically stable model similar to that published by Moreno et al. (1991), who had used a fixed polar grid axisymmetric version of the Los Alamos CAVEAT code. The Michigan code uses an adaptively-refined mesh of square grids. The second more long-range method considered was to make use of the techniques developed for the hybrid gasdynamic-Monte Carlo model for comets (Combi 1989; Combi & Smyth 1988 a&b). This would have combined the hydrodynamic code for the bottom of the atmosphere with a Monte Carlo particle code for the top. In another project we were planning a similar course of action for comet coma modeling.

Since the conception of this project and the original proposal 3 years ago, a number of important and highly relevant studies regarding Io's atmosphere have been published. A number of studies now suggest that only a limited area, perhaps 5-20% of Io's atmosphere is covered by a collisionally thick SO_2 atmosphere--i.e. with surface densities perhaps approaching 10^{11}-10^{12}

cm^{-3} (Lellouch et al. 1992; Sartoretti, McGrath & Parlesce 1994) in the thickest regions. The discovery of the likely molecular ion origin for at least some of Io's fast sodium (Schneider et al. 1991b) implies an abundance of molecules at high altitudes in the atmosphere. Finally, in work performed in a separate project with Dr. William Smyth of AER, Inc., as PI, we (Smyth & Combi 1995) have constructed a consistent model analysis of sodium "eclipse" observations in the corona near Io (surface out to a few Io radii, Schneider et al. 1991a) and the B-cloud emissions (out to ~100 Io radii). The flux distribution for sodium found in Io's atmosphere is best represented by neither a Maxwell-Boltzmann flux distribution nor a classical sputtering distribution. A modified sputtering distribution (also called a collisional cascade distribution) provides an excellent and consistent picture for producing the entire sodium atmosphere out to 100 Io radii.

Strobel et al. (1994) have raised the issue that Joule heating may dominate over plasma impact heating (Johnson 1989; Popieszalska & Johnson 1992). Both processes are really due to the effect of ion-neutral collisions on the atmosphere. In an integrated kinetic model for the atmosphere and ionosphere, as being developed here, the point is moot because the actual microphysical collision description is explicitly included.

The significance of this is that Io's atmosphere at large is neither globally collisionally thick nor near thermal equilibrium, but that collisions are important. Therefore, the application of a hydrodynamic model to describe many aspects of Io's global atmosphere is highly suspect, although it does retain validity if applied in the right regime, such as in the vicinity of the volcano (Moreno et al. 1990).

There have also been other important developments in work not specifically part of this project. In parallel developments, the PI has been working on a fully kinetic Direct Simulation Monte Carlo (DSMC) model for cometary atmospheres, and with colleague Dr. Ronald Miller of the University of Michigan has been working on various aspects of a plasma hybrid kinetic simulation of the Earth's polar wind (Miller & Combi 1994) for the ultimate incorporation of those techniques into an Io model. The DSMC is not the same as the so-called fully kinetic Monte Carlo simulations published by Hodges (1990) or more recently by Xie (1994). The latter are iterative test particle (ITP) methods, which are only applicable to steady-state problems and which require an initial guess for the phase space distribution. A similar ITP model has been applied to the hydrogen exosphere (Hodges 1994). On the other hand, a 1-D radial single species hot oxygen geocorona exosphere model for the Earth using DSMC techniques has been published recently by Shematovich et al. (1994).

In non-equilibrium gas kinetic theory DSMC models have been used to investigate various non-equilibrium aspects of gas flows (such as shock structures, see Bird 1976) for nearly 30 years. DSMC models are inherently time-dependent, and proceed by following the trajectories of many individual molecules, accounting for collisions and other forces. What distinguishes DSMC

from ITP is that DSMC is equivalent to a direct finite difference solution of a time-dependent dilute gas Boltzmann equation description of the system. The ITP method relys on a more heuristic argument of convergence of test particle distribution functions toward the correct distribution functions for each species. They have been shown to give reasonable results in some applications (Bird 1976). However, ITP is not applicable to non-steady flows, such as would be required for understanding system-III variations in the recent HST observations of S and O near Io, which imply variations with the system-III longitude of Io and when Io passes into and out of eclipse (Clarke et al. 1994; Ballester et al. 1994b). The 1-D particle model of Pospieszalska & Johnson (1992) employed a method which is intermediate between ITP and DSMC models, but is also implicitly steady-state.

The PI has engaged Dr. Ronald Miller to collaborate on the Io portion of this project for the purpose of combining an Earth ionosphere polar wind code with neutral gas algorithms developed for the PI's comet modeling program. Dr. Miller, an Assistant Research Scientist in the Space Physics Research Laboratory in collaboration with the PI, is making significant progress toward this original long-term scientific goal at a level of effort of only 2 to 3 months per year because of his expertise in the development and coding of kinetic models and because the projects from which the code is being adapted are already quite mature. Dr. Miller is not new to the Planetary Atmospheres program, having worked with Dr. Tamas Gombosi on cometary ionospheres in recent years.

As of this writing the first version of an axisymmetric 2-D code for Io is near completion. A 1-D spherical version of the kinetic code for a simple hydrostatic equilibrium SO_2 atmosphere has been constructed and tested successfully. Figure 1 shows the density and surface wind field for a 2-D axisymmetric sublimation atmosphere. See the caption for descriptive details. The first coupled ion-neutral kinetic model of the plasma-torus/atmosphere interaction is now undergoing final testing and debugging and a first paper is expected in the first few months of the new project year.

III. References

Bird, G.A. 1976. In "Molecular Gas Dynamics," Academic Press, New York.

Combi, M.R. 1989. The outflow speed of the coma of Halley's comet. *Icarus* **81**, 41-50.

Combi, M.R. 1994. The fragmentation of dust in the inner comae of comets: Possible evidence from ground-based images. *Astron. J.* **108**, 304-312.

Combi, M.R. and U. Fink. 1993. P/Halley: Effects of time-dependent production rates on spatial emission profiles. *Astrophys. J.* **409**, 790-797.

Combi, M., B. Huang, A. Cochran, U. Fink and R. Schulz. 1994. Time-dependent analysis of 8 Days of CN spatial profiles. *Astrophys. J.* **435**, 870-873.

Combi, M.R. and R.H. Miller. 1994. A 2-dimensional kinetic simulation of plasma heating of Io's atmosphere. *EOS*, **75**, (in press).

Combi, M.R. and W.H. Smyth 1988a. Monte Carlo particle trajectory models for neutral cometary gases. I. Models andequations. *Astrophys. J.* **327**, 1026-1043.

Combi, M.R. and W.H. Smyth 1988b. Monte Carlo particle trajectory models for neutral cometary gases. II. The spatial morphology of the Lyman-alpha coma. *Astrophys. J.* **327**, 1044-1059.

Hodges, R.R. 1990. Monte Carlo simulation of nonadiabatic expansion in cometary atmospheres: Halley. *Icarus* **83**, 410-433.

Lellouch, E. et al. 1992. The structure, stability, and global distribution of Io's atmosphere. *Icarus* **98**, 271-295.

Miller, R.H. and M.R. Combi 1994. A Coulomb collision algorithm for weighted particle simulations. *Geophys. Res. Let.* **21**, 1735-1738.

Moreno, M.A.,G. Schubert, J. Baumgardner, M.G. Kivelson, and D.A. Page. 1991. Io's volcanic and sublimation atmospheres. *Icarus* **93**, 63-81.

Pospieszalska, M.K. and R.E. Johnson. Plasma heating of Io's atmosphere. *Geophys. Res. Let.* **19**, 949-952.

Sartoretti, P. M.A. McGrath and F. Paresce. 1994. Disk-resolved imaging of Io with the Hubble Space Telescope. *Icarus* **108**, 272-284.

Smyth, W.H. and M.R. Combi. 1994. Io's sodium corona and spatially extended cloud: A consistent flux speed distribution. *Icarus* (submitted).

Schneider, N.M. et al. 1991. Molecular origin of Io's fast sodium. *Science* **253**, 1394-1397.

Smyth, W.H., M.L. Marconi, M.R. Combi. 1994. Analysis of hydrogen Lyman-alpha observations of the coma of comet P/Halley near perihelion. *Icarus* 113, 119-128.

Xie, X. 1993. Ph.D. Thesis, University of Pennsylvania

Xie, X. and M. Mumma. 1993. Presented at Asteroids, Comets, Meteors 1993, in Belgirate, Italy June 14-19, 1993.

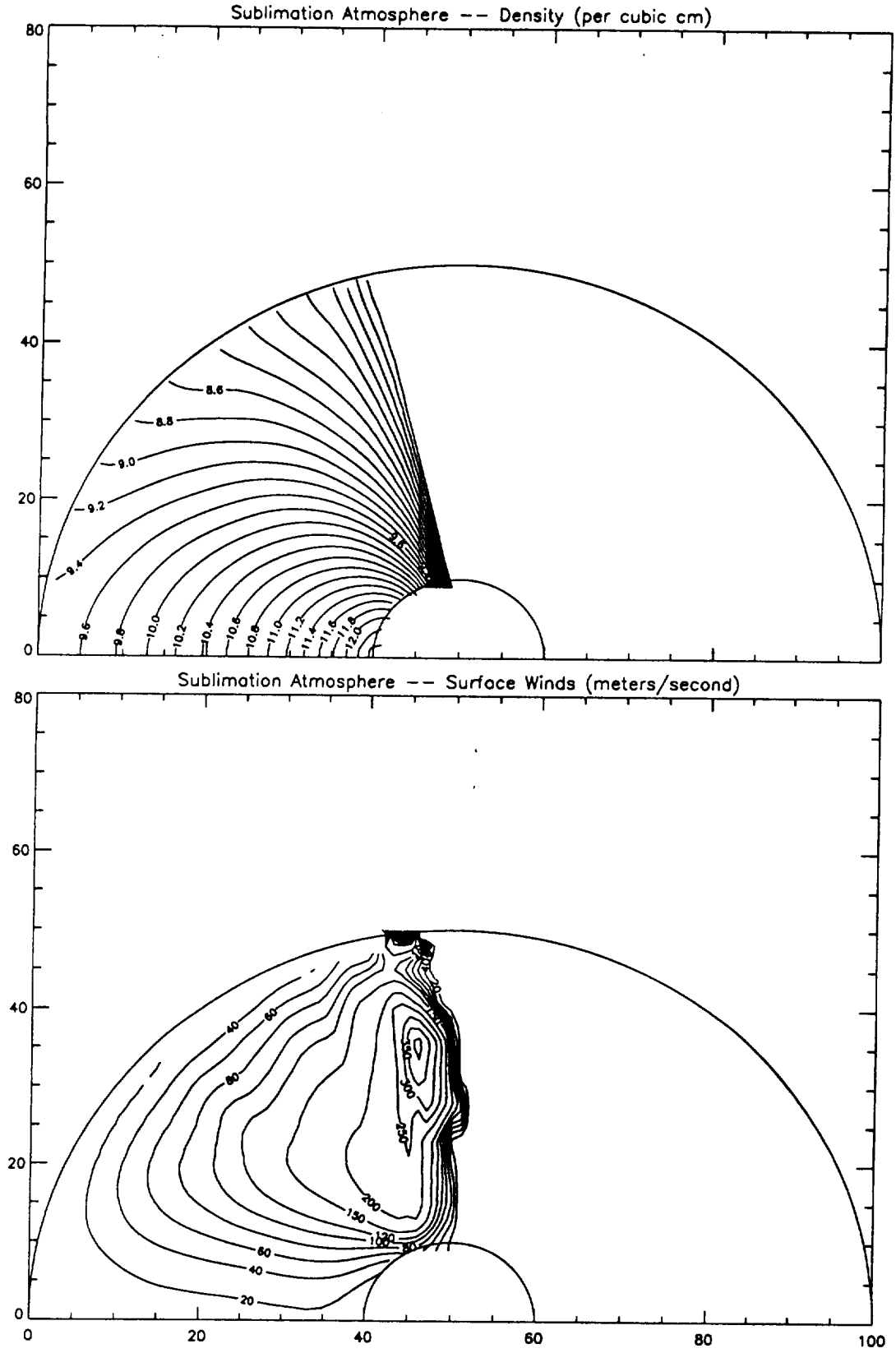

Figure 1. 2D-Axisymmetric Kinetic Model for Io's Sublimation Atmosphere. Shown are contour plots for SO_2 density (above) and horizontal winds (below). The small circle at the bottom is Io's radius (1820 km). The lower horizontal axis is the symmetry axis with the Sun to the left. The radial scale has been stretched so that the large circle corresponds to an altitude of 80 km. At low altitudes and near the subsolar point the density and surface winds are similar to hydrodynamic models. The kinetic model is valid for high altitudes and subsolar angles $>60^{o}$ where fluid models are invalid.

APPENDIX

THE FRAGMENTATION OF DUST IN THE INNERMOST COMAE OF COMETS: POSSIBLE EVIDENCE FROM GROUND-BASED IMAGES

MICHAEL R. COMBI

Space Physics Research Laboratory, Department of Atmospheric, Oceanic and Space Sciences, University of Michigan, Ann Arbor, Michigan 48109-2143

Electronic mail: combi@sprlc.sprl.umich.edu

Received 1994 January 11; revised 1994 February 25

ABSTRACT

Dust particles when released from the nucleus of a comet are entrained in the expanding gas flow created by the vaporization of ices (mainly water ice). Traditional approaches to dusty-gas dynamics in the inner comae of comets consider there to be an initial distribution of dust particle sizes which do not fragment or evaporate. The standard Finson–Probstein model (and subsequent variations) yields a *one-to-one-to-one* correspondence between the size of a dust particle, its terminal velocity owing to gas drag, and its radiation pressure acceleration which creates the notable cometary dust tail. The comparison of a newly developed dust coma model shows that the typical elongated shapes of isophotes in the dust comae of comets on the scale of $>10^4$ km from the nucleus requires that the one-to-one-to-one relationship between particle size, terminal velocity and radiation pressure acceleration cannot in general be correct. There must be a broad range of particles including those having a small velocity but large radiation pressure acceleration in order to explain the elongated shape. A straightforward way to create such a distribution is if particle fragmentation, or some combination of fragmentation with vaporization, routinely occurs within and/or just outside of the dusty-gas dynamic acceleration region (i.e., up to several hundred km). In this way initially large particles, which are accelerated to fairly slow velocities by gas-drag, fragment to form small particles which still move slowly but are subject to a relatively large radiation pressure acceleration. Fragmentation has already been suggested as one possible interpretation for the flattened gradient in the spatial profiles of dust extracted from Giotto images of Comet Halley. Grain vaporization has been suggested as a possible spatially extended source of coma gases. The general elongated isophote shapes seen in ground-based images for many years represents another possible signature of fragmentation.

1. INTRODUCTION

The standard dust coma treatments originated with the pioneering work of Finson & Probstein (1968a,b) which considers the dust to consist of a population of particles having a variation of sizes with a size distribution determined by a power law in particle diameter. The particles were considered to have a constant density, $\rho(a)=\rho_0$, independent of particle size. The light scattering properties which are needed not only to describe the observed scattered radiation but also to calculate the radiation pressure acceleration on each particle size were considered to be simply proportional to the geometric cross section of the particle implying that the light scattering efficiency, Q_{scat}, and the radiation pressure efficiency, η_{rp}, both equal unity and are independent of particle size. It is clear from the work of a number of investigators that these underlying assumptions are highly oversimplified for physical dark absorbing dust particles (e.g., see the excellent review by Grün & Jessberger 1991).

Jewitt & Luu (1990) have published the results of a Monte Carlo dust coma model applied to observations of Comet P/Tempel 2. Their model is steady state and spherical. Ellis & Neff (1991) have developed a numerical dust model for neutral or charged dust for comparison with dust experiments on Vega 1 and 2 and Giotto. However, their results state that the dust particle terminal velocities required to match their model to data are 1.7 times the values implied by conventionally dusty-gas dynamics. The resulting dust velocities would exceed the velocity of the gas that is accelerating the dust. This seems implausible.

Baum *et al.* (1992) have presented a number of models compared with CCD images of comets, however their fountain model upon which they base some of their analysis is incorrect owing to a subtle error in their derivation which actually had been shown correctly in an old paper by Wallace & Miller (1958) as well as in a similar but slightly more complicated form by Haser (1966). In their Fig. 5(a), Baum *et al.* show a model result for a point source with constant radiation pressure which shows isophote contours that, while not elongated, appear to be circles drifting tailward. On the contrary, the results of Wallace & Miller (1958) shown in their Eq. (8) and in the upper left portion their Fig. 3, clearly state "that, for any position of the observer whatever, the isophotes are circles with center at the nucleus, or arcs of circles terminated by the (projected paraboloid) envelope," and "the intensity is inversely proportional to the radius of the isophote." However, the conclusion of Baum *et al.*, that some dust particles seem to decay with scale lengths on the order of magnitude of $\sim 10^5$ km, is not dependent on this aspect of their model and is consistent with some of the Giotto data (see the review by Sekanina 1987).

The Finson–Probstein method has generally been applied

to wide-field images of the large-scale dust tail (Finson & Probstein 1968b; Sekanina & Miller 1973). The dust coma within about 10^5 km from the nucleus presents a different challenge. Fulle (1987) introduced a Monte Carlo approach to the Finson–Probstein inversion method which permitted relieving some of the restrictive simplifying assumptions. Most recently Waniak (1992) has published the results of using a similar Monte Carlo approach to the inversion method where the calculation was extended to spatially anisotropic emission from the nucleus.

In this paper a dust coma model is presented which is based on the Monte Carlo techniques previously applied to gas species in cometary atmospheres (Combi & Delsemme 1980; Combi & Smyth 1988a) and which is fully time dependent and three dimensional. The light scattering efficiency, radiation pressure efficiencies, and dust particle densities are allowed to take on physically realistic values that vary with particle size. Such complexities as anisotropic sources, periodically varying production rates, and particle fragmentation and decay have been incorporated into the model for comparison with data. Anisotropic emission and periodically varying production rates have been addressed with this model in previous preliminary studies (Combi & Fink 1992). The general objective of constructing such a model is to compare it with some of the wealth of CCD images of the dust coma (as opposed to the dust tail), that are available for Comet Halley, in order to explore the possibility of seeing visible effects of important physical processes.

In this paper the shapes of modeled isophote shapes of the coma are compared with those detected in the typical field of view ($\sim 10^5$ km) afforded by a CCD camera and a fairly large telescope. Section 2 of this paper presents the mathematical description of the basic model. Section 3 presents a comparison of the standard model with a representative set of narrowband continuum images of Comet Halley taken during the pre-perihelion period. Section 4 discusses a heuristic dust fragmentation model which can faithfully reproduce the shapes of the observed isophotes, for different viewing geometries and conditions. And finally, Sec. 5 presents a discussion and summary of results.

2. A GENERAL DUST COMA MODEL

The basic framework of our dust model is built on the basis of the hydrogen coma model discussed in detail in the papers by Combi & Smyth (1988a,b). It is a fully 3D time-dependent Monte Carlo particle trajectory model that builds up an entire coma by following the trajectories of many individual particles. For the published gas coma model, the particles are individual atoms, radicals, and molecules; for the dust model the particles are obviously individual dust particles. The mathematical treatment for many of the basic processes, namely the angular dispersion of initial trajectories, time-dependent production rate, heliocentric trajectory calculations with solar gravity and radiation pressure, collection of particle weights for the calculation of column densities, etc., has already been described in great detail in the above papers and will not be discussed further here. What will be discussed here are those aspects of the model which are unique to the dust model: the physical properties of the dust particles, their size distribution and density, terminal dusty-gasdynamic velocities, light scattering, and radiation pressure efficiency.

From polarization measurements of Comet Halley (Mukai *et al.* 1987) it is clear that cometary grains have similar optical properties of a material commonly called astronomical silicate: i.e., a dark dielectric. Although that real cometary grains are not expected to be spherical but may be quite irregular, the adoption of Mie theory which assumes spherical particles has proven to be quite useful by other investigators. The results of Mie calculations by Hoban *et al.* (1989) have been adopted for the light scattering properties in our model.

Hellmich & Schwehm (1984) calculated the radiation pressure efficiency as a function of size for dark dielectric material, which is believed to be indicative of cometary dust particles. The radiation pressure efficiency drops precipitously for very small particles and peaks for particles whose sizes are in the range of the wavelength of the peak of the solar radiation. This calculation has been adopted for the standard radiation pressure efficiency in the model.

Probably more uncertain than the question of gross optical properties of small dark grains in this problem are their densities. Although it has been traditional to assume densities of 1 to 3 g cm^{-3}, it is likely that cometary grains are porous aggregates and therefore have a density which decreases with increasing radius. Lamy *et al.* (1987) have suggested a dust density of the form

$$\rho(a) = 2.2 - 1.4a/(a_0 + a), \tag{1}$$

where a = particle radius and $a_0 = 2$ microns. This has been chosen as a starting point for the modeling studies presented here. They can be easily scaled, although the dependence on size for aggregate particles must at least be qualitatively correct. Note that the dust denstity function in Eq. (1) has the same form as that used by Gombosi (1986) [$\rho(a) = 3.0 - 2.2a/(a_0 + a)$] but the dust densities are uniformly somewhat smaller.

For the differential dust production rate the Hanner-type distribution of Gombosi (1986) has been adopted which gives

$$\frac{dz_d(a)}{da} = \frac{4\pi}{3} a_0^3 \rho_a \varphi_0 \frac{x^k}{(1+x^2)}, \tag{2}$$

where a = dust particle radius,

$z_d(a)$ = the cumulative dust mass production rate in particles per unit time,

$dz_d(a)/da$ = the dust mass production rate for particles with radii between a and $a + da$,

a_0 = a parameter taken to be 2 microns,

$x = a/a_0$,

ρ_a = density of dust particles of size a, and

ϕ_0 = a normalization constant which is set by the integrated dust production rate.

It is related to the gas production rate with the proportionality constant χ, such that $z_d(a_{\max}) = Q_d = \chi Q_g$, and $z_d(a_{\min}) = 0$, where $a_{\min}$ and $a_{\max}$ are the smallest dust particle sizes in the distribution.

The value of k is taken to be 1.5 (Gombosi 1986). The size distribution function of dust particles produced yields a function of the form $a^{-(3.2 \text{ to } 3.6)}$, where the exponent has a slightly smaller magnitude (3.2) for the smallest particles and somewhat larger (3.6) for the largest particles, so as to be in agreement with various *in situ* studies (McDonnell *et al.* 1991) and with comet tail studies (Waniak 1992, and Fulle *et al.* 1988 for Halley; and Fulle 1987 and 1988 for other comets).

For the particle velocities the best approach is the dusty-gas dynamic method initially developed by Probstein (1968) and subsequently improved (see Wallis 1982; Marconi & Mendis 1983; Gombosi *et al.* 1985) to include the feedback of drag by the dust on the gas flow. Sekanina (Sekanina 1981; Sekanina & Larson 1983) has developed a simple empirical method for computing dust particle velocities in a gas flow which accounts for the mass loading on the gas flow, the gas production rate, and the dust-to-gas mass ratio. Since our purpose is to generate an explicitly time-dependent dust model, having a fast approximate alternative to having to do a quasi-time-dependent treatment by running many individual full dusty-gas dynamic models is of great benefit. In any case, any errors introduced by Sekanina's approximation are, on the whole, much smaller than those introducted by the uncertainties in the other physical details and assumptions of the model.

In Sekanina's approximation the velocity of dust particles with radius, a, is given by

$$v_a = v_g \left[\frac{1}{3} \left(1 + \frac{0.65}{1+\alpha(a)^{2/3}} \right) (1 + 0.38\chi^{0.6}) + 0.225\alpha(a)^{1/2} \right], \quad (3)$$

where v_g=gas velocity in the dust acceleration region ($\sim$0.42 km s^{-1}),

$\alpha(a) = [c v_g \eta_{rp}(a)]/[R_n Z \beta(a)]$,

$c\beta = 1.83 \times 10^{-4}$ g cm^{-2},

χ=dust-to-gas mass ratio,

$\beta(a) = [c\beta\eta_{rp}]/[\rho_a a]$,

η_{rp}=radiation pressure efficiency,

ρ_a=dust particle density [Eq. (1)],

$c\beta = 0.585 \times 10^{-4}$ g cm^{-2},

$Z = Q_g/4\pi R_n^2$, the vaporization rate per unit surface area,

Q_g=gas production rate, and

R_n=radius of the nucleus ($\sim$6 km for Halley).

Comparisons of the results of using Eq. (3) with the explicit dusty-gas dynamic model results of Gombosi *et al.* (1986) show excellent agreement across the entire particle size distribution and for the complete range of gas production rates relevant for Halley.

For the long term secular dependence of the dust production rate, those determined in the photometry of Schleicher and co-workers (Schleicher 1993) of $r^{-2.3}$ for pre-perihelion and $r^{-1.9}$ for post-perihelion, where r is the heliocentric distance of the comet have been adopted. Preliminary results of adopting the 7.4 day periodic variation seen in comet Halley (Schleicher *et al.* 1990) and anisotropic coma emission have already been explored using this new dust model (Combi & Fink 1992).

TABLE 1. Observational parameters.

Date (UT)	Exposure (s)	R (AU)	Δ (AU)	Phase (°)
1985 Nov 9.2529	300	1.82	0.89	15.1
1985 Dec 4.0302	300	1.45	0.66	36.0
1985 Dec 27.9694	300	1.08	1.06	54.6

3. COMPARISON OF MODELS WITH DUST COMA IMAGES

A set of CCD images of Comet P/Halley were made using the 61 in. Wyeth telescope at the Oak Ridge Observatory, of the Havard-Smithsonian Center for Astrophysics from September through December 1985. The standard IAU comet filter set with wavelengths centered at 3840 Å (CN), 4280 Å (CO^+), 4840 Å (continuum), 5160 Å (C_2), 6840 Å (continuum) and 7130 Å (H_2O^+) was used and various comet, flux-calibrated star, and flatfield exposures were taken. Unfortunately, an unpredictable failure of the camera shutter (a sticky shutter) was discovered much later after a considerable effort was made to calibrate the images using standard star images and understand the inconsistent results. However, the combination of the flatfield and "continuum" images do yield images of the dust coma distribution, albeit uncalibrated, that are still quite useful. Comparison of several pairs of nearly simultaneous 6840 and 4840 Å images show that there appears to be no major difference in the image gradients that could be attributable to the wavelength difference (i.e., indicative of some particle size discrimination) so the rest of the analysis is based upon the 6840 Å images which had a much better signal-to-noise ratio because of the better sensitivity of the overall system at that wavelength.

Table 1 gives the pertinent information for the 6840 Å images analyzed for this paper. A contour plot display of one of the images is shown Fig. 1. Immediately noticeable is that the apparent radiation pressure acceleration produces progressively more elongated isophotes in the tailward direction with increasing distance from the nucleus. This is reminiscent of many other bright comets [see, for example, the isophotometric atlas of Högner & Richter (1969)]. In this respect the isophote shapes are similar to the H Lyman-α images of a number of comets (Meier *et al.* 1976; Opal & Carruthers 1977; Smyth *et al.* 1991). On the contrary, a comparable model image, shown in Fig. 2, tends to give more circular isophotes which terminate rather abruptly in the sunward direction. The comparison is drawn with the H coma images because the reasons for the shape, both the immediate phenomenological reason and the ultimate physical cause are understood in the case of cometary hydrogen, and thus serves as a guide for understanding the similar shape of the dust coma.

Work by Keller and co-workers (Keller & Meier 1976) showed that the elongated isophotes seen in the H comae of comets required that the H atoms emitted from the inner coma possess a broad distribution in speeds away from the

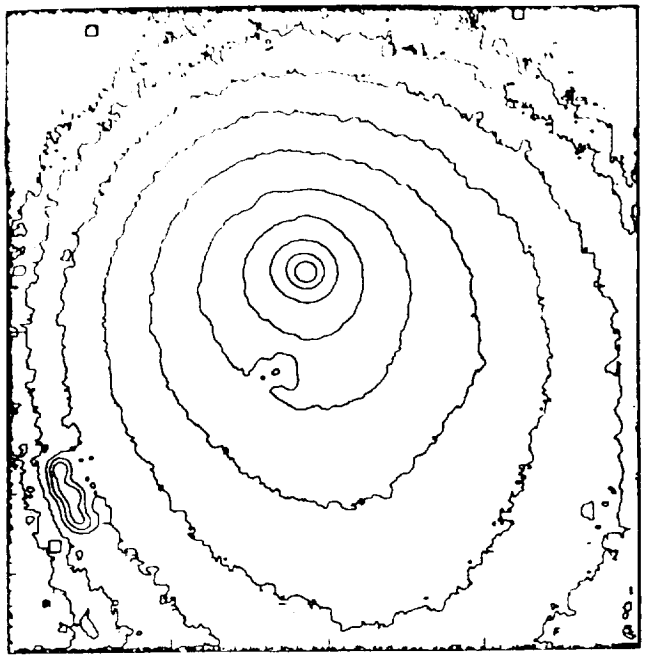

FIG. 1. A 6840 Å narrowband CCD image of Comet P/Halley on 1985 December 4. Shown is a contour plot of a 6840 Å Halley Watch filtered image of Comet P/Halley taken with the 60 in. Wyeth telescope at the Harvard/Smithsonian Oak Ridge Observatory. The image has been corrected for flatfield deviations but is not intensity calibrated. The linear dimension of the square image is 1.398×10^5 km and the Sun is clearly to the upper left. Note especially the elongated shapes of the contours toward the tail direction.

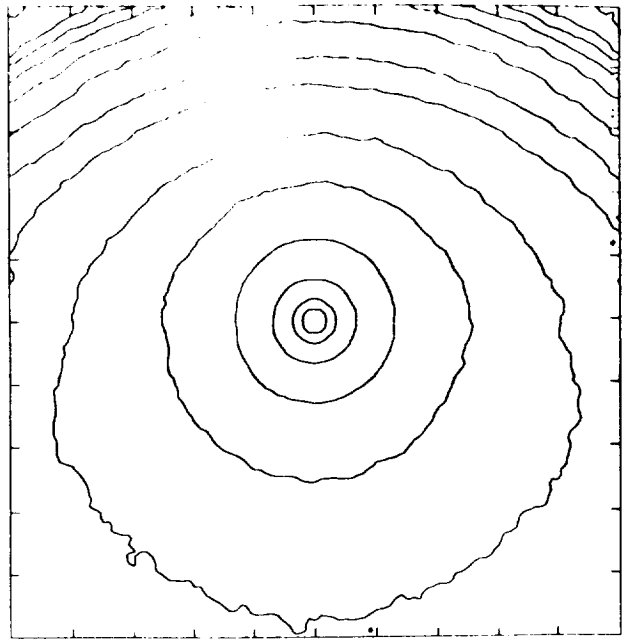

FIG. 2. Standard dust model for Comet Halley on 1985 December 4. A surface brightness contour plot is shown for the standard model (no fragmentation) as discussed in Sec. 2. The Sun is up. Note in comparison with the data image in Fig. 1 that, although the magnitude of the solar radiation pressure induced distortion is approximately correct, the model contours are much more round than the elongated contours in the data in the tailward direction. Other data images are similarly elongated. The model consisted of 1,000,000 dust particles in each of 28 logarithmically distributed size bins from 10^{-7} to 10^{2} cm.

nucleus. As discussed in Sec. 1 of this paper, Wallace & Miller (1958), building on work begun with the original fountain model of Eddington (1910), showed that for a simple point source emission subject to a constant acceleration in one direction, the resulting "coma" falls within a paraboloid of revolution, and that isophote distribution appears to be circles that are centered on the nucleus *for all viewing geometries*. In order to build up a more realistic coma, a distribution of particles having a range of radiation pressures and/or outflow velocities would be required. Figure 3 illustrates the appearance of such a single component point source model with radiation pressure. In many ways, is it not unlike the appearance of the much more complicated dust model shown in Fig. 2, despite the addition of a dust particle size distribution. Certainly the isophote contours are not elongated in the tailward direction as they appear in observed images such as Fig. 1.

In the analogous case of the Lyman-α coma, the value of the radiation pressure acceleration on H atoms is nearly constant, and only very weakly dependent on the somewhat different heliocentric velocities of individual atoms. A distribution in velocity was found by Keller to be required to produce the rather elongated tailward coma seen at large distances. This can be thought of as a superposition of many Wallace and Miller point source paraboloids. (This discussion of course ignores the effect of the relative solar orbits between various particles and the nucleus which would distort the simple point source model, but the basic character is still the same. The dust coma model presented here does include this effect.) A distribution in speeds, formed from the sum of three Maxwellian distributions (at 4, 8, and 20 km s^{-1}), provided a good reproduction of the isophote maps of comet Kohoutek (1973 XII). Later, Combi & Smyth (1988b) showed that the combination of photodissociation of H_2O and OH combined with partial collisional thermalization of the H atoms in the inner coma produced a broad

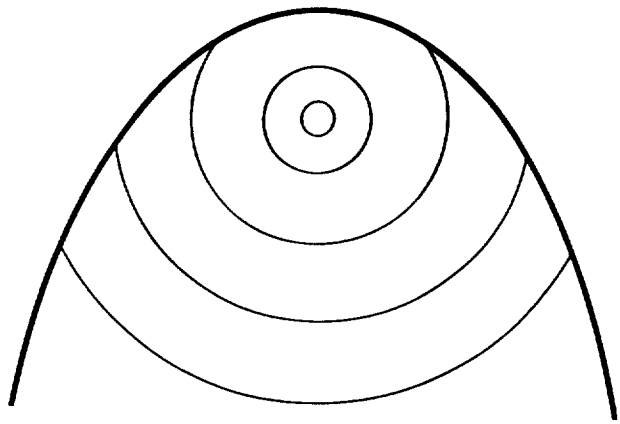

FIG. 3. Point-source model isophote contour map. The appearance of the simple point-source model with radiation pressure of Wallace & Miller (1958) is illustrated. Note that the isophote contours are circular and centered on the position of the nucleus. They end discontinuously at the position of the projected paraboloid of revolution whose vertex distance is given by $v^2/2b$, where the value, v, is the outflow speed and the value, b, is the radiation pressure acceleration.

distribution of H atom velocities leaving the inner ($< 10^5$ km) coma, similar to but more irregular than Keller's Maxwellians. This new distribution also provided a good reproduction of the isophote shapes. This time, however, the model contained few adjustable parameters, and the speed distribution was the straightforward (but complicated) result of the actual physical and chemical processes in the coma.

For dust particles there is a similar problem. Since the radiation pressure acceleration and the outflow speed (i.e., terminal velocity) of a certain size dust grain depend in a similar way on the geometrical cross section and density, one finds that there is only a fairly narrow range of the quantity $v^2/2b$, where "v" is the initial radial velocity of a dust particle and "b" is its acceleration, among the particles which contribute to most of the total scattered light when integrating over the abundance-weighted cross section. If the particle velocities are increased or decreased by factors of two, the resulting coma stills shows rather circular isophotes, similar to the simple Wallace and Miller point source paraboloid shape, albeit with a larger or smaller paraboloid envelope. A similar effect can be obtained if the size distribution or the density is changed.

Finally, an unusual initial angular distribution of dust from the nucleus cannot produce elongated isophotes, except possibly for an antisunward "beam" of dust which just does not make physical sense. Various exploratory models have been run in connection with this paper and the previous work of Combi & Fink (1992), and in none of these cases does one obtain tailward-elongated isophotes. Other single velocity anisotropic and sunward-throwing point source models appear in the paper by Wallace & Miller (1958) and there is nothing there to indicate that one could obtain tailward-elongated isophotes by some sunward ejection distribution of dust. The last argument against a source distribution producing the elongation is the fact that it is clearly present in all images, with different observing geometry and presumably various configurations of active regions on the sunward hemisphere.

In the case of the H coma, radial outflow speeds ranging from 1 to more than 20 km s^{-1}, and all having about the same radiation pressure acceleration, are required in order to produce the elongated isophotes which are observed. In order to produce similar elongated isophotes for dust, a similar spread in velocities for certain values of the radiation pressure acceleration would be required. As mentioned earlier, provided that dust particles leave the nucleus with certain sizes and remain those sizes, dusty-gas dynamics requires that for each size (and density) that a single terminal velocity will be obtained. One way to account for a variation in speed for particles of a certain size is if the acceleration were more of a stochastic process (as in molecular collisions). However, given the large size of dust particles relative to gas molecules, the fluid-drag approach does seem valid. Another mechanism which would produce a range in velocities for each particle size would be if there were large scale fragmentation of dust particles within 1000 km from the nucleus. The major acceleration occurs within the first several nucleus-radii, whereas most ground-based images have pixel resolutions corresponding to ~1000 km. If large dust particles are initially accelerated to rather small velocities by the gas drag and then subsequently fragment to smaller sizes, the newly created and slowly moving small fragments would be subject to relatively large radiation pressure accelerations. This fragmentation process would produce a broad continuum of particle velocities for each particle size, and thus produce the kind of source needed to account for elongate isophotes. Such fragmentation has been suggested by Thomas & Keller (1990) and Konno *et al.* (1993) to explain various aspects of the Giotto Halley Multicolor Camera observations of the very inner coma of comet Halley. Here, it is suggested that there is clear evidence for large scale fragmentation in the typical ground-based observatory images of the comae of bright comets which have been available for many years.

4. A HEURSTIC DUST FRAGMENTATION MODEL

To model fragmentation in a rigorous way would require a full dusty-gas dynamic treatment, where an original distribution of dust particle sizes are initially liberated from the nucleus, and the physics of the fragmentation process is prescribed. Konno *et al.* (1993) have done something like this in their 1D steady-state model, where they prescribe a certain rate of fragmentation from an initial distribution of particles to a set of discrete smaller sizes. However, although thermal stress and the dust acceleration process have been suggested as likely sources for fragmentation, a real physical description of the fragmentation process has never been attempted.

For the purpose of reproducing images, a simple and adjustable parametrized method is required. It is assumed that an initial particle of radius, a, is accelerated to the value determined by the Sekanina approximation of dusty-gas dynamics. Since the model is already Monte Carlo based, Monte Carlo methods have been used to fragment the particles. If the particle fragments, then some collection of particles such that $a_f < a$ will result. If an initial particle of radius, a, in the absence of particle vaporization (i.e., producing gas molecules rather fragmentation into smaller dust particles), is broken up into equal sized particles of radius, a_f, then by conservation of mass the number of smaller particles will equal

$$N = \frac{a^3 \rho}{a_f^3 \rho_f} . \tag{4}$$

If all possible fragment sizes were equally probable then a suitable distribution of fragmented particles of radius, a_f, originating from initial particles of radius, a, could be obtained using $a_f = aR_i$ where R_i is a random number on the interval from 0 to 1. Since this is not necessarily so, an adjustable parameter, p, is introduced such that the new particle radius is chosen as

$$a_f = aR_i^p . \tag{5}$$

Such a form can be skewed to favoring smaller or larger particles (i.e., more or less fragmentation) by letting p take on any value greater than or equal to zero. Zero of course would yield the original distribution, that is, no fragmentation.

Figure 4 shows the effect of variation of the fragmentation parameter, p, on the shapes of the isophotes for the same model already shown in Figure 2. The isophotes become elongated in the tailward direction just as in the case of the H coma. As p gets larger, more smaller particles are produced from initially large ones, and the isophotes become more elongated in the tailward (anti-sunward) direction. Figure 5 shows a comparison of three observed images with the model having $p = 2.0$, which provides the best match. Values of 1.5 and 2.5 are not as good. Not only are the projected isophotes the correct shape but both the general scale of the sunward–antisunward asymmetry and the radial profile are also reasonably well reproduced.

The reproduction by the model is certainly not perfect, but nor is it yet meant to be. The images of December 4 and 27 clearly show effects of sunward-enhanced ejection of dust which are not included in the model. In addition, the outer isophote in the tailward direction in the December 27 (to the lower left) is more extended in the model than in the data. Changing the fragmentation parameter does not effect the scale of the sunward–tailward distortion as much as it effects the shapes of the isophotes making them more pointed in the tailward direction. On the other hand, the inclusion of a sunward-enhanced ejection of dust would have the effect of suppressing the tailward gradient relative to the sunward gradient while still preserving the tailward pointed shape indicative of the effect of fragmentation. Such exploration of the very large available parameter space to also investigate spatial anisotropy, short-term time-dependent variations, as well as values of the other dust parameters described in the basic model in Sec. 2 will be the focus of future work.

5. DISCUSSION AND SUMMARY

Althought the heuristic dust fragmentation distribution is certainly not meant to be a unique solution for the detailed dust size–velocity distribution, the fact that it can reproduce the elongated isophotes, where the standard dust models having the 1-to-1-to-1 correspondence between size, velocity, and radiation pressure acceleration cannot, does indicate that this correspondence cannot in general be correct. That fragmentation occurs in the innermost coma has been suggested from the Giotto images (Thomas & Keller 1990; Konno *et al.* 1993). Thomas and Keller in particular found that each original dust particle must fragment into at least 2.7 daughter particles. The value implied for the fragmentation parameter, p, of 2.0, which best reproduces the shape of the dust isophote contours, implies a much larger rate of ~60 daughter particles per parent particle.

There is, however, a caveat regarding the large rate of fragmentation implied here. The optical range CCD images show the distribution of particles in the size range as small as only about one-tenth of a micron. The many small particles detected in Halley by *in situ* dust instruments (Sekanina 1987) have a very small radiation scattering efficiency and are essentially invisible in optical images. This is the reason why early attempts at using the Finson–Probstein method yielded a small particle size cutoff in the vicinity of 0.1–0.3 μm (see Sekanina & Miller 1973). Because of this, the va-

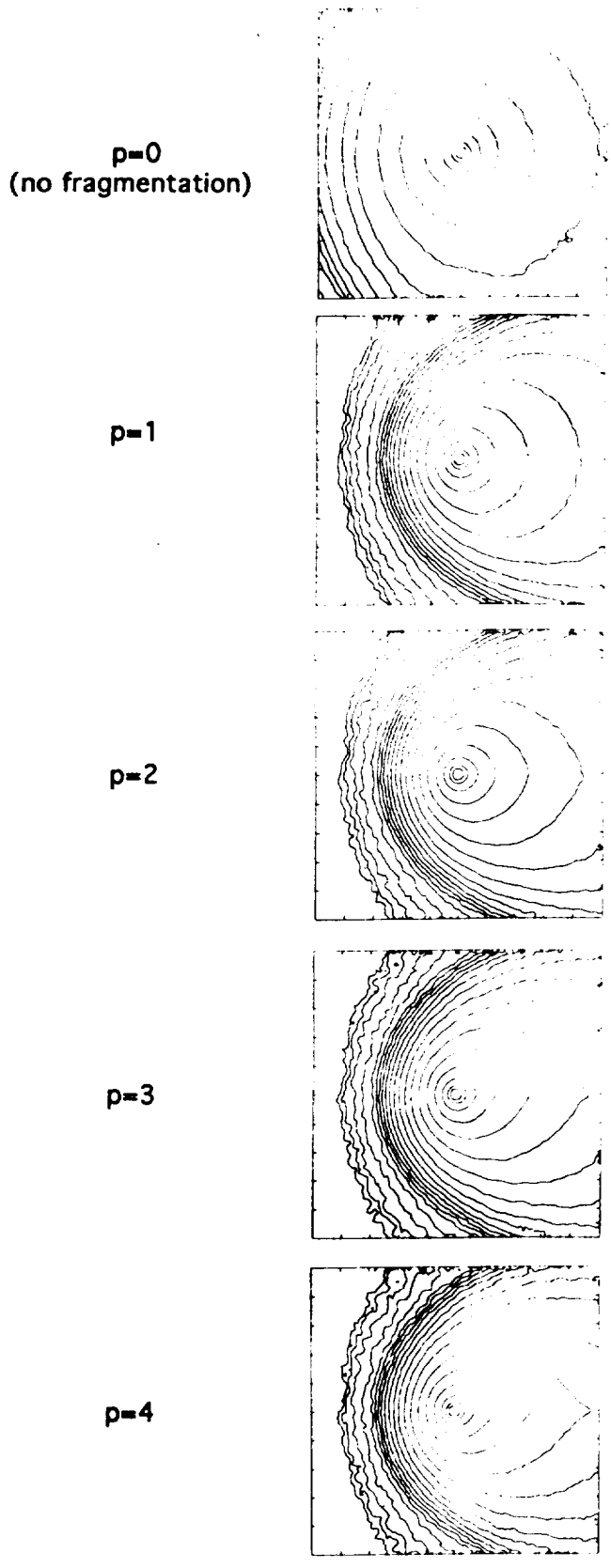

FIG. 4. Variation of the shape of the dust coma with the amount of dust fragmentation. The modeled dust coma for the 1985 December 4 image of Comet Halley is shown for dust fragmentation parameters of 0 (no fragmentation), 1, 2, 3, and 4. Models have been run for values at the half-integer values. A value of 2.0 provides the best reproduction of isophote contour shape. Contour intervals correspond to factors of two in surface brightness.

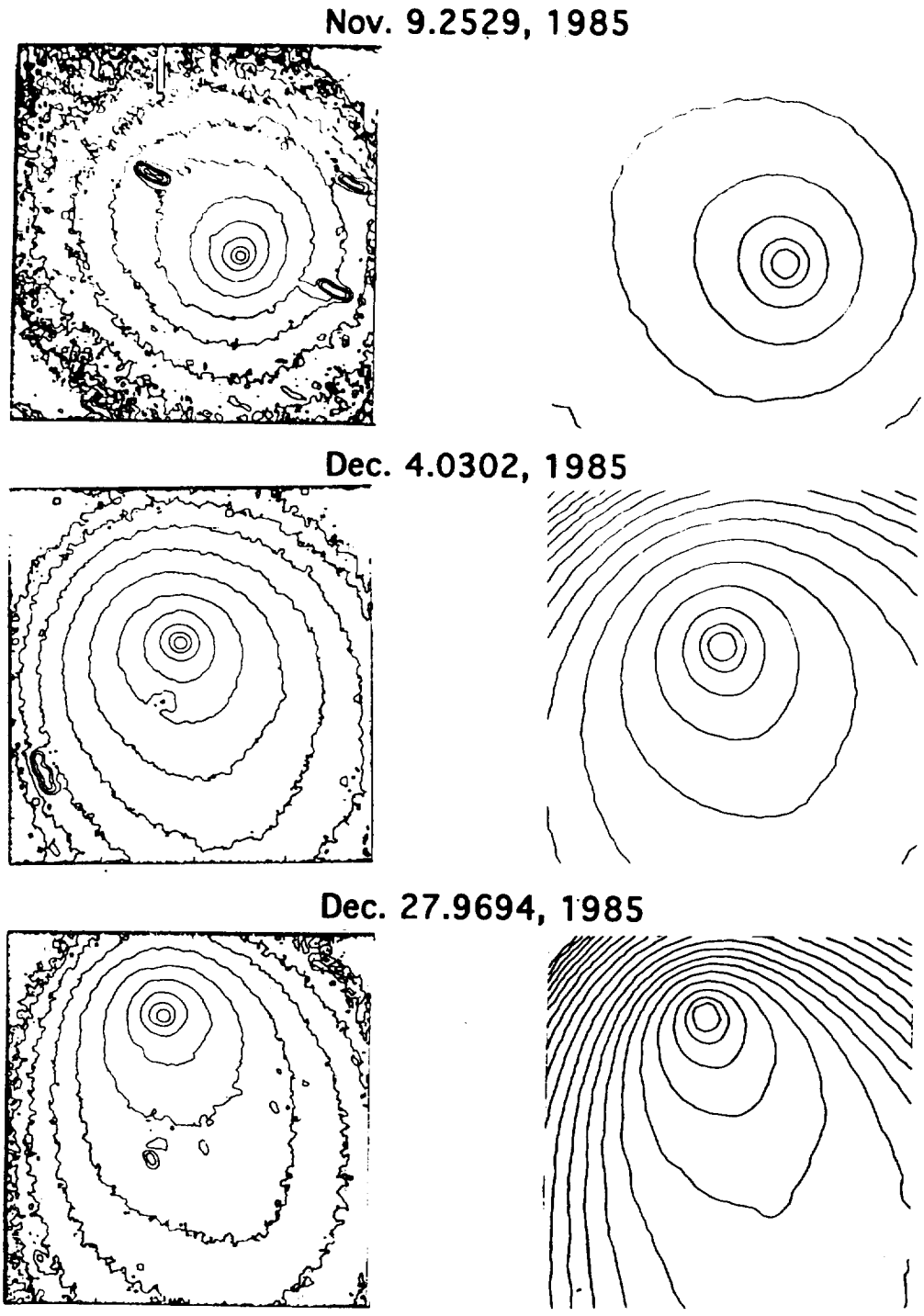

FIG. 5. Comparison of the dust fragmentation model with CCD images of Comet P/Halley. On the left are shown contour plots of three 6840 Å images of Comet P/Halley on the dates indicated. On the right are the corresponding best-fit models with a fragmentation parameter equal, p, equal to 2.0. Note that adjacent contour levels are separated by a factor of two. Slightly preferential sunward ejection of dust is seen in the observed image on 27 December. No attempt to fit this asymmetry for the analysis is presented here. Note that in the observations, there is some error in relative positions of the outermost contours caused by the uncertainty in the level of the sky background which was taken as the value in one of the sunward most corners of each image where the signal was the lowest. Somewhat smaller values improve the agreement in the contour positioning compared with the model. In any case, the shape of the isophote contours are not effected by the background uncertainty. Finally, there are more inner contours in the data images since the data pixel size is 400×400 whereas the model grid resolution is only 100×100. The linear dimensions of the images from top to bottom are 1.840×10^5, 1.398×10^5, and 2.287×10^5 km, respectively.

lidity of the fragmentation function cannot be extended to much below a tenth of a micron. Whereas the fragmentation function is providing a reasonable picture of the velocity/size distribution of particles as small as 0.1 μm, it could very well be overproducing many much smaller particles, which are for all purposes invisible. Unfortunately, images at optical wavelengths can provide no constraint on the very small particles. Therefore, the fragmentation rate of 60 daughter

particles per parent particle may be better thought of as an upper limit.

Since this framentation process conserves mass, something very close to the original $a^{-3.2-3.6}$ distribution remains, in agreement with *in situ* studies (McDonnell *et al.* 1991). The initial distribution, before fragmentation, includes very large particles (1 m), and so the final distribution is complete by any definition below about 0.1 m, since particles this large do not contribute much to the total scattered light in the visual dust coma. If an appreciable fraction of the grain mass were liberated as a gas in a fragmentation/vaporization process, i.e., if there is grain vaporization in addition to grain fragmentation, then it could be treated simply as a loss fraction. If the loss were independent of initial particle size, then something close to the same original and final distributions would remain. If not, then a very different initial particle size distribution might be required, in order to yield the "observed" distribution as a by-product.

The CCD images of Baum *et al.* (1992) provided evidence for grain fading, i.e., a departure from $1/\rho$ in the isophotes, in 10 out of 14 comets they observed. This fading was explained either by a decrease in the albedo or the size (more likely) of particles with time. Combi & Fink (1992) reported that, at least for the case of P/Halley, any departures from $1/\rho$ were understood in terms of the well-known time varying production rate and did not require grain fading. Fading of the very small, suboptical grains could of course occur without effecting the appearance of optical images.

The fragmentation of dust particles (Thomas & Keller 1990; Konno *et al.* 1993) has the opposite effect of fading on the radial profile, since as particles break apart, the total surface area of all the small particles is larger than that of the original large particles. On the contrary, fading or vaporization of large grains into small grains via the production of gas produces a smaller total surface area in the resultant small particles since the number of particles is conserved. Although, the analysis of the ground-based images in this paper cannot *per se* distinguish between fragmentation and vaporization as the primary source of the required slow and small grains, the appearance of the flatter than $1/\rho$ distribution in the Giotto HMC images in the immediate vicinity of the nucleus would seem to favor fragmentation being dominant over vaporization. Since dust-to-gas mass ratios are thought to be of order unity, certainly 10% of the dust mass could be lost to vaporization, and explain an additional extended source of gas, whereas 90% of initially large dust grains could fragment into many smaller dust grains, and still substantially increase the total scattering surface are, thereby producing the required flat radial profile.

Fragmentation and vaporization of dust particles in the region immediately surrounding the nucleus have been suggested to be a possible mechanism for expanding the subsonic flow region, isotropicizing the day-side source, serving as an extended source of gas, and being responsible for the surface breeze that sends dust directly to the night-side of the coma very near the nucleus (Keller *et al.* 1990). Clearly the combination of fragmentation and vaporization of dust in the innermost comae of comets may be one of the most important mechanisms for explaining a number of poorly understood phenomena in comets.

Further lines of important study in this area are the more careful analysis of more dust coma and tail images of comets with a fragmentation model, and the two- and three-dimensional modeling of dusty-gas flows with dust fragmentation and vaporization. Future applications of the dust model presented here will include dust coma and tail image analyses with anisotropic ejection models [done in preliminary fashion already by Combi & Fink (1992)], as well as more careful study of the constraints (or lack thereof) presented by the small (sub-optical) grains.

The unpublished narrowband CCD images of Comet P/Halley shown here were taken and reduced by Dr. Richard E. McCrosky (Harvard/Smithsonian), who in turn thanks GTE Research Laboratories for instrumentation support to Oak Ridge Observatory. The critical reading by an anonymous referee and helpful suggestions is gratefully acknowledged. Support for this work was provided by Grant No. NASW-1908 and NAGW-3417 from the Planetary Atmospheres program.

REFERENCES

Baum, W. A., Kreidl, T. J., & Schleicher, D. G. 1992, AJ, 104, 1216
Combi, M. R. 1989, Icarus, 81, 41
Combi, M. R., & Delsemme, A. H. 1980, ApJ, 237, 633
Combi, M. R., & Fink, U. 1992, BAAS, 24, 1018
Combi, M. R., & Smyth, W. H. 1988a, ApJ, 327, 1026
Combi, M. R., & Smyth, W. H. 1988b, ApJ, 327, 1044
Eddington, A. S. 1910, MNRAS, 70, 442
Ellis, T. A., & Neff, J. S. 1991, Icarus, 91, 280
Finson, M. L., & Probstein, R. F. 1968a, ApJ, 154, 327
Finson, M. L., & Probstein, R. F. 1968b, ApJ, 154, 353
Fulle, M. 1987, A&A, 171, 327
Fulle, M. 1988, A&A, 189, 281
Fulle, M., Barbieri, C., & Cremonese, G. 1988, A&A, 201, 362
Gombosi, T. I. 1986, in 20th ESLAB Symposium on the Exploration of Halley's Comet, edited by B. Battrick, E. J. Rolfe, and R. Reinhard, ESA SP-250, II, pp. 167–171
Gombosi, T. I., Cravens, T. E., & Nagy, A. F. 1985, ApJ, 293, 328
Gombosi, T. I., Nagy, A. F., & Cravens, T. E. 1986, Rev. Geophys. 24, 667
Grün, E., & Jessberger, E. 1991, in the Physics and Chemistry of Comets, edited by Walter Huebner (Springer, New York), pp. 113–176
Haser, L. 1966, Mem. Soc. Roy. Soc. Liege, Ser. 5, 12, 233
Hellmich, R., & Schwehm, G. H. 1984, in Cometary Exploration, edited by T. I. Gombosi (Central Research Institute for Physics, Hungarian Academy of Sciences, Budapest) III, pp. 175–183
Hoban, S., A'Hearn, M. F., Birch, R. V., & Martin, R. 1989, Icarus, 79, 145
Högner, W., & Richter, N. 1969, Isophotometric Atlas of Comets (Barth, Leipzig)
Jewitt, D., & Luu, J. 1990, AJ, 97, 1766
Keller, H. U., Marconi, M. L., & Thomas, N. 1990, A&A, 227, L1
Keller, H. U., & Meier, R. R. 1976, A&A, 23, 269
Keller, H. U., *et al.* 1987, A&A, 187, 807
Konno, I., Huebner, W. F., & Boice, D. C. 1993, Icarus, 101, 84
Lamy, P. L., Grün, E., & Perrin, J. M. 1987, A&A, 187, 767
Marconi, M. L., & Mendis, D. A. 1983, ApJ, 273, 381

McDonnell, J. A. M., Lamy, P. L., & Pankiewicz, G. S. 1991, in Comets in the Post-Halley Era, edited by R. L. Newburn, Jr., M. Neugebauer, and J. Rahe (Kluwer, Dordrecht), pp. 1043–1073
Meier, R. R., Opal, C. B., Keller, H. U., Page, T. L., & Carruthers, G. R. 1976, A&A, 52, 283
Mukai, S., Mukai, T., & Kikuchi, S. 1987, A&A, 187, 650
Opal, C. B., & Carruthers, G. R. 1977, Icarus, 31, 503
Probstein, R. F. 1968, in Problems of Hydrodynamics and Continuum Mechanics (Society for Industrial and Applied Mathematics, Philadelphia, PA), p. 568
Schleicher, D. G. 1993, private communication
Schleicher, D. G., Millis, R. L., Thompson, D. T., Birch, P. V., Martin, R., Tholen, D. J., Piscatelli, R., & Lark, N. L. 1988, AJ, 100, 896
Sekanina, Z. 1981, AJ, 86, 1741
Sekanina, Z. 1987, A&A, 187, 789
Sekanina, Z., & Larson, S. M. 1984, AJ, 89, 1408
Sekanina, Z., & Miller, F. D. 1973, Science, 179, 565
Smyth, W. H., Combi, M. R., & Stewart, A. I. F. 1991, Science, 253, 1008
Thomas, N., & Keller, H. U. 1991, A&A, 249, 258
Wallace, L. V., & Miller, F. D. 1958, AJ, 63, 213
Wallis, M. K. 1982, in Comets, edited by L. L. Wilkening (University of Arizona Press, Tucson, AZ), pp. 357–369
Waniak, W. 1992, Icarus, 100, 154

THE ASTROPHYSICAL JOURNAL, 435:870–873, 1994 November 10

TIME-DEPENDENT ANALYSIS OF 8 DAYS OF CN SPATIAL PROFILES IN COMET P/HALLEY

MICHAEL COMBI AND BORMIN HUANG
Space Physics Research Laboratory, University of Michigan, 2455 Hayward Street, Ann Arbor, MI 48109-2143. combi@sprlc.sprl.umich.edu
ANITA COCHRAN
Astronomy Department, University of Texas, Austin, TX 78712
UWE FINK
Lunar and Planetary Laboratory, University of Arizona, Tucson, AZ 85721
AND
RITA SCHULZ
Max-Planck-Institut für Aeronomie, Max-Planck-Strasse 2, D-37191 Katlenburg-Lindau, Germany
Received 1994 March 7; accepted 1994 May 9

ABSTRACT

CN profiles in comet P/Halley were constructed from observations taken at three observatories during an 8 day period in April 1986. These data provide a time series of CN spatial profiles spanning just over one 7.37 day period from 1986 April 7 to April 15 and sample distances from the nucleus from just over 10^3 km to 10^6 km. The effect of the 7.37 day periodic variation on the CN distribution in P/Halley has been examined by using the time-dependent model applied earlier to a subset of the data. Because of the large spatial scale of the data on April 7, 8, and 9 ($\sim 10^6$ km), and the corresponding transport time in the coma, information present in the spatial profiles regarding the gas production rate actually covers nearly two full periods. These spatially extended profiles clearly show the wavy structures outside 10^5 km. Such structures were predicted in a previous analysis (Combi & Fink 1993) that was based solely on the photometric light curve and on profiles which only extended to distances less than 10^5 km. We are now able to reproduce the highly variable Halley CN profiles using the same model as before, with the same standard scale lengths, phase lag, and amplitude correction for the variation in gas production rate.

Subject heading: comets: individual (Halley)

1. INTRODUCTION

In the earlier comprehensive studies of spatial profiles of the molecular species, CN and C_2, in comets, Combi & Delsemme (1980, 1986) warned of the influence of the irregular time variation of the parent gas production rate on the shapes of the profiles and its influence on dissociation scale lengths extracted from those profiles. Their conclusion was that, provided many spatial profiles taken at different times are included and that fitted scale lengths (using Haser's model) or lifetimes (using vectorial or Monte Carlo models) are treated in a *statistical* manner, the effect of gas producton rate could be, in a sense, averaged out. This was borned out by the results of Fink, Combi, & DiSanti (1991), whose Haser model analyses of observations of spatial profiles in comet Halley were generally consistent *on the average* with those of other comets, despite the now well-known large amplitude periodic variation in the postperihelion period (Schleicher et al. 1990).

Although the detailed nature of the compound rotational motion of the nucleus of Halley's comet is not known for certain (Samarasinha & A'Hearn 1991; Belton et al. 1992), it is clear that throughout its active period, and especially during the postperihelion period, the rotational motion caused a variation in gas and dust production with a period between 7.3 and 7.6 days (Millis & Schleicher 1986; Schleicher et al. 1990). The effect of the periodically varying gas production rate was demonstrated by Combi & Fink (1993) in spatial profiles of CN, C_2, NH_2 and O(^{1}D) taken on 1986 March 1 and 2 and April 14 and 15 by a model based on the photometric light curve of Schleicher et al. (1990). All profiles covered radial distances of less than 10^5 km, and so each only sampled just over 1 day of cometary activity out of the total 7.37 day period. Furthermore, the profiles predicted a continuation of wavy structures in the profiles which should continue out to large distances (10^6 km) and have detectable changes with time.

In this paper we present an analysis of spatial profiles of CN in comet P/Halley constructed from observations that were taken at three observatories and covering 8 days, from 1986 April 7 through April 15. Because of the large spatial scale ($\sim 10^6$ km) of the data from the early part of this period, and given the transport times from the nucleus to these distances, the data actually contain information about two full 7.37 day periods. The model of Combi & Fink (1993) with the same parameters for the scale lengths and the phase lag and amplitude correction to the photometric light curve can reproduce the structure in all the profiles. This paper first describes that observational data, then the model analysis and results, followed lastly by a discussion and conclusions.

2. OBSERVATIONS

Spatial profiles of the CN (0–0) band of the violet system and the (1–0) band of the red system were collected from three separate observing campaigns and are summarized along with the Comet Halley's geometry in Table 1. Data were obtained from ESO/LaSilla, McDonald Observatory of the University of Texas, and the Lunar and Planetary Laboratory of the University of Arizona. For simplicity, the three data sets will be referred to as ESO, MCD, and LPL, respectively, in the remainder of this paper.

TABLE 1

SPATIAL PROFILES OF CN IN COMET P/HALLEY

Date (UT 1986)	R (AU)	Δ (AU)	Site[a]	Profile Orientation
April 7.09[a]	1.27	0.44	ESO	Perpendicular
April 8.09	1.29	0.43	ESO	Perpendicular
April 9.14	1.30	0.42	ESO	Perpendicular
April 10.40	1.32	0.42	MCD	Sun/tail
April 14.3	1.38	0.43	LPL	Sun/tail
April 15.3	1.39	0.44	LPL	Sun/tail

NOTES.—R is the heliocentric distance in AU, Δ is the geocentric distance in AU, Sun/tail refers to the average of spatial profile along the sunward and tailward directions of the comet-Sun line, and perpendicular refers to the spatial profile perpendicular to projection of comet-Sun line.

[a] ESO is ESO/LaSilla, MCD is McDonald Observatory, and LPL is University of Arizona.

The data for April 7, 8, and 9 (ESO) were constructed from wide-field filtered photographic images of the comet taken by the Bochum Halley Monitoring Program at ESO. The data were taken with an f/4 Lichtenknecker Flat-Field Camera with a focal length of 760 mm and a corresponding field of view of 1°8 by 2°7. They were digitized with a PDS microdensitometer and calibrated for relative intensity using spot sensitometry. Other details regarding these data and their reduction have already been published (Celnik et al. 1988; Schulz & Schlosser 1990; Schulz 1992).

The profile from April 10 was constructed from long-slit spatial-spectral images obtained with a 512 × 320 pixel RCA CCD with the Large Cassegrain Spectrograph on the 2.7 m telescope MCD. The original spectra covered wavelengths from 3650–6800 Å. The slit was 2".1 wide for most of the observations. A pixel corresponded to 1".3, but observations in the outer coma were binned to 2".6 to improve the signal-to-noise ratio. Seven separate observations were made, stepping the slit through the coma by computer control of the telescope. The general data set and more details regarding the observations have already been published elsewhere (Cochran & Cochran 1990).

We include here for completeness the two CN profiles of April 14 and 15 (LPL), already analyzed in the previous paper by Combi & Fink (1993). These data were obtained from long-slit CCD spectra covering wavelengths of 5000–10,000 Å that were taken with the 154 cm Catalina Site Telescope of the University of Arizona Observatories. Contrary to the above data, these correspond to the (1–0) band of the CN red system at 9200 Å. The observations, data reduction, and construction of spatial profiles have already been presented in detail by Fink et al. (1991). Their paper points out the agreement between spatial profiles taken in mid-December of the (1–0) red system with those of the (0–0) violet system which appear in the paper of Cochran & Barker (1986). Therefore, it is clear that the red and violet systems can both be used to construct spatial profiles, although the violet system does provide more signal and far less background from dust-continuum and night-sky contamination.

Although an absolute calibration for the spatially integrated long-slit spectra is now available (Fink 1994), none was used for the spatial profiles (Fink et al. 1991). The MCD and ESO data had their own separate calibrations. However, intercomparison between the data revealed that some of the absolute calibrations were suspect, especially those obtained at very large zenith angles (large air mass). Because of this, we obtained CN column densities from Schleicher (1992) which are updates and more complete than those originally published by Millis & Schleicher (1986).

A confusion zone close to the nucleus is present in the spatially resolved data and is caused by the unpredictability of guiding and seeing with slit or aperture size and averaged over the source region of the coma where brightness gradients are large. Because of this, we chose to calibrate the spatial profiles by using the difference between pairs of small and large aperture photometric observations. The two aperture sizes were typically about 80" and 150" in diameter. The difference in the column abundances between two such apertures yields the total abundance in an annulus with inner radius equal to the small aperture and outer radius equal to the larger one. Each radial profile was then treated as if it were in arbitrary units and integrated numerically around an annulus of the same size, assuming the distribution was circular. The ratio between the photometric abundances and the spatial profile integral yielded a simple calibration factor, S, for each spatial profile, which is given as

$$S = \frac{M_{A_L} - M_{A_S}}{2\pi \int_{A_S}^{A_L} \rho B(\rho) d\rho},$$

where M_{A_L} is the number of molecules in larger aperture, M_{A_S} is the number of molecules in smaller aperture, ρ is the projected distance from the nucleus, $B(\rho)$ is the brightness as a function of ρ, and M_{A_L} and M_{A_S} are obtained from the photometry (Schleicher 1992). Since the IHW photometry net collected data from around the world, there were high-quality photometric observations obtained within minutes of each of the spatial profiles. The photometry results used in our absolute calibration is listed in Table 2.

When this scaling was done for the already calibrated MCD and ESO data, values ranged from 1 to 2 even after accounting

TABLE 2

RESULTS OF CN PHOTOMETRY USED IN ABSOLUTE CALIBRATION OF SPATIAL PROFILES

Data (UT 1986)	log ρ[a] (km)	log g[b] (ergs s^{-1})	log M[c]
April 7.092	4.09	−12.473	30.62
April 7.098	4.39	...	31.13
April 8.079	4.08	−12.472	30.72
April 8.112	4.38	...	31.16
April 8.283	4.08	−12.473	30.75
April 8.290	4.38	...	31.20
April 9.117	4.07	−12.473	30.77
April 9.140	4.37	...	31.23
April 10.395	4.07	−12.474	30.51
April 10.401	4.37	...	31.01
April 14.352	4.08	−12.475	30.54
April 14.374	4.38	...	31.05
April 15.296	4.09	−12.476	30.60
April 15.305	4.39	...	31.01

NOTE.—Information in this table was provided by Schleicher 1993.

[a] The term ρ is the radius of the photometric aperture.

[b] The g-factor is the radiative emission rate for CN(0–0) reduced to 1 AU in ergs s^{-1}.

[c] M is the number of CN radicals within the aperture.

for differences in adopted g-factors. In theory, all values should have been unity. However, the use of standard observatory extinction curves at high air masses, rather than measured ones, and observing at unusually high air mass made the internal calibrations very uncertain in two cases. The consistent external calibration of all spatial profiles using the annuli from the photometric observations yielded excellent results. It should be mentioned that the analysis presented here is sensitive to the relative calibration between the spatial profile data rather than the absolute calibration per se. It was clear that there was a relative calibration problem between the independently calibrated spatial profile data sets which were alleviated by the use of the photometric data set.

3. MODEL ANALYSIS AND RESULTS

The results of Combi & Fink (1993) showed that a time-dependent model constructed with Monte Carlo methods and the photometric light curves of Schleicher et al. (1990) could reproduce pairs of profiles for four molecular species in comet Halley on March 1 and 2 and April 14 and 15. The standard March and April light curves of Schleicher et al. (1990) had to be shifted in time, implying an expected phase lag between the activity at the comet nucleus and observed changes in the large photometric aperture. The light curve also had to be "decompressed" because the amplitude seen in the photometry is compressed both by aperture integration and by the extended source nature of producing daughter species, as compared with the amplitude of the variation of the parent gas production source. For April data, a phase lag of 6 hr and an amplitude correction of 27% was found to be required for all four species in question, CN, C_2, NH_2 and O(^{1}D).

For the analysis in this paper we simply tried the same model parameters for the times (i.e., the phases of the periodic variation) that each of the new observations were made. In the previous analysis of 2 adjacent days of data, the change in production rate owing to the long-term variation with heliocentric distance ($r^{-2.39}$ postperihelion), that Schleicher et al. (1990) had divided out of their results before finding the periodic variation, yielded only a small shift ($\sim$2%) between data from 2 adjacent days. For the 8 days of data presented here, this long-term variation yields a 25% ramp down in the production rate from April 7 to April 15. This had to be taken into account for this analysis, the results of which are shown in Figure 1.

The points are the data, and the lines are the model results. The absolute scale of the column density corresponds to the top profile from April 7. All of the others, both model and data, are shifted down by factors of 3 in column density for clear examination. The results for April 14 and 15 are the same as those described earlier by Combi & Fink (1993), except for the small scaling factor which accounts for the long-term production rate variation. Clearly, the wavy features seen at large distances, in the range from 10^5 to 10^6 km from the nucleus, as predicted in the published models, are evident in the data from April 7, 8, and 9. It should be stressed that there was no independent adjustment for each profile. The relative positioning of all model profiles with all observed profiles was locked as a group.

4. DISCUSSION

The general shapes and variations of the observed profiles are well reproduced by the model, but are not perfect. There are a number of reasons why some deviations should be

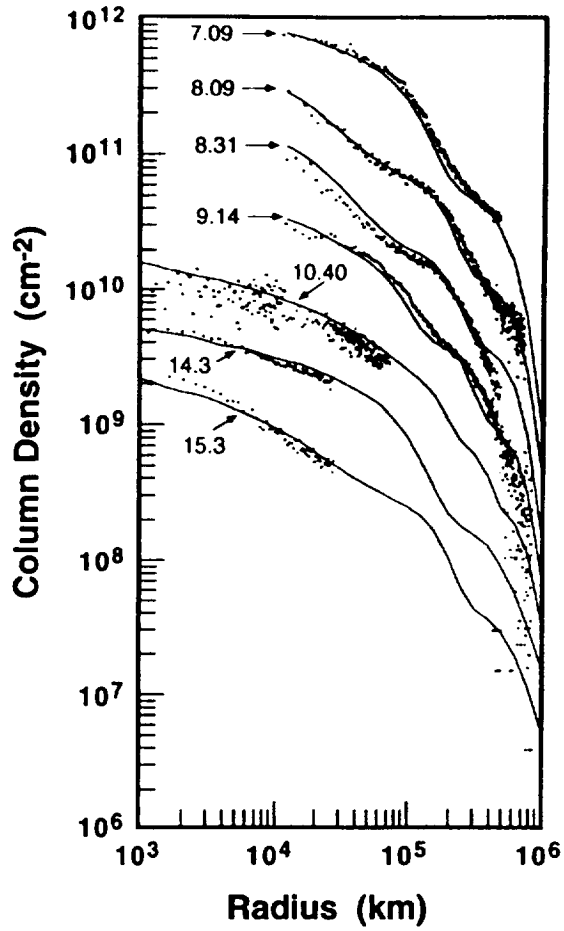

FIG. 1.—Comparison of 8 days of CN spatial profiles with the time-dependent model. The points give the observed radial profiles covering the period from April 7 through April 15 (*from top to bottom*). The lines correspond to the model of Combi & Fink (1993). The column density scale corresponds to the first (April 7.09) profile and each subsequent one (both data and model) is shifted downward by a factor of 3 below the one above so they can be distinguished.

expected. The model is a Haser-like time-dependent model, so all CN radicals have radially outflowing velocities. In reality there will be some dispersion caused by the "vectorial" ejection of radicals when produced from the parent molecules (or grains). At times closer to perihelion, when coma densities were larger and dissociation lifetimes shorter, more radicals would have been produced well within the collision zone where much of this excess velocity from dissociation would have been collisionally quenched (see, for example, the OH models results of Combi, Bos, & Smyth 1993). The fact that radicals will then have some range of velocities as they move away from the nucleus then implies that the peaks and troughs of the variation (as in a wave propagation) should be compressed at larger distances from the nucleus. The model does not include this effect, so this behavior is apparent in the model-data comparison.

The CN radicals seen at distances of 10^6 km from the nucleus on April 7 were produced as part of a parent molecules and/or grains 12 days earlier, near March 26 when the heliocentric distance was 1.1 AU, as compared with 1.3 AU in mid-April. Furthermore, the production rates and corresponding coma outflow speeds were higher at earlier times. There is

evidence in the model-data comparison that the wave structures have propagated a bit farther out in the data compared with the model. This could be explained by this expected variation in outflow speed. It is also clear from the original photometric data base that every 7.4 day period of activity was not identical to every other (Schleicher et al. 1990), so some real differences are probably present since the model is based on the shape of an average light curve.

Finally, it should be mentioned that the model is obviously spherically symmetric and does not make an attempt to distinguish between CN jets (A'Hearn et al. 1986) and CN background (Klavetter & A'Hearn 1992, 1994). Deviations from circularity were apparent in some of the spatial profiles in opposite directions, but these have been averaged out by averaging radial profiles on opposite sides of the nucleus.

In order to analyze wide-field spatial profiles or images covering distances out to 10^6 km, it will be necessary to make use of a completely time-dependent calculation which accounts for both long- and short-term variations in production rate and for long-term variations in photochemical lifetimes and radiation pressure acceleration. This would be akin to a heavy radical version of the hydrogen coma model constructed to analyze wide-field Lyα images of comets (Combi & Smyth 1988). Although the typical spatial scales of those images are an order of magnitude larger, the H velocities are also an order of magnitude larger, so the problems are quite scalable.

As mentioned above, the one-dimensional profile data presented here do not contain any information regarding the angular distribution of material ejected from localized areas on the rotating nucleus. This particular isotropic model analysis of these data is not sensitive to any changes in the spatial orientation of active areas and therefore cannot provide any discrimination between alternative nucleus models. It should be noted, however, that the 7 day periodically varying light curve (Schleicher et al. 1990), which is used as the basis of our time-dependent model, is also one of the important data sets contributing to the phasing and period of the nucleus models (Samarasinha & A'Hearn 1991; Belton et al. 1992).

The results presented here do indicate that it may be possible to use a more complicated model to analyze a large set of two-dimensional images in order to test the complex rotational motions in the alternative models of the nucleus. This would not be without some further model assumptions, though, since the flow physics responsible for producing the coma that is somewhat isotropicized from what appear to be obviously localized sources on the sunward side of the nucleus (Keller, Marconi, & Thomas 1990) is not yet understood. Fragmentation and continued vaporization of dust have been suggested as a possible source for day-to-night side breezes which could inject some dust directly into the night-side hemisphere and would also be an obvious explanation for the somewhat isotropicized (Klavetter & A'Hearn 1994) gas flow in the coma.

Finally, since the use of simple time-dependent models with standard average parameters (scale lengths and lifetimes, velocities) can reproduce spatial profiles which are otherwise shaped by variable production rates, as in the periodic cases of Halley, P/Swift-Tuttle, or Levy (1990c), then a single or limited set of spatial profiles could be used to generate the light curve of cometary activity with the appropriate inversion technique.

We thank D. Schleicher for providing the latest version of the CN column densities from his latest unpublished compilation of the International Halley Watch photometry, which were used for the absolute calibration. Support to the University of Michigan was provided by grant NASW-3417 from the NASA Planetary Atmospheres program. Support for the ESO/LaSilla observations was provided by Deutsche Forschungsgemeinschaft.

REFERENCES

A'Hearn, M. F., Hoban, S., Birch, P. V., Bowers, C., Martin, R., & Klinglesmith, D. A., III. 1986, Nature, 324, 649
Belton, M. J. S., Julian, W. H., Anderson, A. J., & Mueller, B. E. A. 1992, Icarus, 93, 183
Celnik, W. E., Koczet, P., Schlosser, W., Schulz, R., Svedja, P., & Weissbauer, K. 1988, A&AS, 72, 89
Cochran, A. L., & Barker, E. S. 1986, in Exploration of Halley's Comet (ESA SP-230), 439
Cochran, A. L., & Cochran, W. D. 1990, in Proc. Workshop, Observations of Recent Comets, ed. W. F. Huebner et al. (San Antonio: Southwest Research Institute), 22
Combi, M. R., Bos, B. J., & Smyth, W. H. 1993, ApJ, 408, 668
Combi, M. R., & Delsemme, A. H. 1980, ApJ, 237, 641
———. 1986, ApJ, 308, 472
Combi, M. R., & Fink, U. 1993, ApJ, 409, 790
Combi, M. R., & Smyth, W. H. 1988, ApJ, 327, 1044
Fink, U. 1994, ApJ, 423, 461
Fink, U., Combi, M. R., & DiSanti, M. A. 1991, ApJ, 383, 371
Keller, H. U., Marconi, M. L., & Thomas, N. 1990, A&A, 227, L1
Klavetter, J. J., & A'Hearn, M. F. 1992, Icarus, 95, 73
———. 1994, Icarus, in press
Millis, R. L., & Schleicher, D. G. 1986, Nature, 324, 646
Samarasinha, N. H., & A'Hearn, M. F. 1991, Icarus, 93, 194
Schleicher, D. G. 1992, private communication
Schleicher, D. G., Millis, R. L., Thompson, D. T., Birch, P. V., Martin, R., Tholen, D. J., Piscatelli, R., & Lark, N. L. 1990, AJ, 100, 896
Schulz, R. 1992, A&A, 268, 319
Schulz, R., & Schlosser, W. 1990, Proc. 24th ESLAB Symp. on the Formation of Stars and Planets, and the Evolution of the Solar System (ESA SP-315), 121

ICARUS 113, 119–128 (1995)

Analysis of Hydrogen Lyman-α Observations of the Coma of Comet P/Halley near Perihelion

WILLIAM H. SMYTH AND M. L. MARCONI

Atmospheric and Environmental Research, Inc., Cambridge, Massachusetts 02139
E-mail: smyth@aer.com

AND

MICHAEL R. COMBI

Space Physics Research Laboratory, University of Michigan, Ann Arbor, Michigan 48109

Received October 7, 1993; revised August 29, 1994

The Pioneer Venus Orbiter Ultraviolet Spectrometer measurements of the Lyman-α intensity of atomic hydrogen excited by solar resonance scattering in the coma of Comet P/Halley acquired from December 28, 1985, to January 6, 1986, and from January 31, 1986, to March 6, 1986, are simulated with the Monte Carlo Particle Trajectory Model corrected for optical depth effects. Spatially detailed comparisons between data and model show excellent agreement and are used to infer that the highest cometary activity may not be at perihelion, but about 2½ weeks before. An improved set of H_2O production rates is presented for the period of time that the spectrometer was observing and is found to be consistent with the rates from other types of measurements. The apparent discrepancy between Stewart (1987, *Astron. Astrophys.* 187, 369–374) in early March and International Ultraviolet Explorer OH derived rates is resolved. The problem with the conversion of 18-cm OH radio brightnesses to H_2O production rates is also discussed.

1. INTRODUCTION

The 1986 passage of Comet Halley through perihelion was received with an unprecedented observational effort. Between September 1985 and June 1986, Comet Halley was the target of long-term systematic observations by multiple groundbased and orbit based facilities as well as *in situ* measurements by five flyby missions. Observations were carried out from the radio to the ultraviolet. Part of the vigorous program was the Pioneer Venus Orbiter Ultraviolet Spectrometer (PVOUVS) observations of solar Lyman-α resonantly scattered from the hydrogen in the coma of Halley. Due to the proximity of Halley to the Sun in the terrestrial sky, only PVOUVS Lyman-α and OH 18-cm radio measurements of Halley could be taken near perihelion. Since the OH brightness radio measurements for large production rates such as occurred for Halley near perihelion are not easily interpreted, the PVOUVS data attain particular importance. As a result, although Stewart (1987) already analyzed the PVOUVS data, here the data are reexamined with a significantly improved approach.

Stewart (1987) studied the data using a Haser model, neglecting the optical thickness of the hydrogen coma in Lyman-α and utilizing a brightness which represented a spatial average centered on the brightest point of the data. However, as shown in Smyth *et al.* (1991) and also below in this paper, optical depth corrections are quite substantial near the brightest point. In addition, the spatial averaging of the data by Stewart (1987) eliminated valuable spatial information, and the scale of averaging by early March 1986 was so large (5×10^6 km by 8×10^6 km) that temporal resolution was also compromised. Nevertheless, Stewart's H_2O production rates seem reasonable overall, with the only apparent discrepancy occurring in early March when the International Ultraviolet Explorer (IUE) OH measurements (Combi *et al.* 1993) indicate a much lower rate.

In this article the Monte Carlo Particle Trajectory Model (MCPTM), which has been used very successfully to study various other data sets such as IUE measurements for OH (Combi *et al.* 1993) and H (Combi and Feldman 1992, 1993) and groundbased measurements for Hα (Smyth *et al.* 1993) as well as O(^{1}D) and NH_2 (Smyth *et al.* 1995), is adopted. As discussed below, the MCPTM attempts to treat properly the dynamics and chemistry of cometary hydrogen. The MCPTM is additionally corrected for optical thickness effects, and as shown in Smyth *et al.* (1991) as well as here, it is able to accurately simulate the spatial brightness distribution from PVOUVS. Consequently, it is possible to extract information about the temporal history of the water produc-

0019-1035/95 $6.00

tion from a single observation so that even the PVOUVS data gap (January 7 to January 30) is accessible to analysis. Moreover, the examination of the early March data can be undertaken on substantially smaller spatial scales ($\sim 2 \times 10^6$ km) than in the analysis of Stewart (1987).

In this paper, the MCPTM corrected for optical depth effects is used to validate the ability of the model to accurately describe the distribution of hydrogen in the coma of Halley, to extract an improved set of H_2O production rates for the PVOUVS observation period, and to obtain some information of the level of cometary activity during the period January 10 to January 30, where only OH radio measurements cover the entire interval. The observational data are described in Section 2, followed by the modeling analysis in Section 3. In Section 4, model results are discussed, and conclusions from the analysis are presented.

2. OBSERVATIONS AND DATA

A comprehensive description of the observations and data is given in Stewart (1987). Here we shall summarize the most relevant points of that description. Comet Halley was systematically observed by the PVOUVS at various wavelengths including Lyman-α from December 28, 1985, to January 6, 1986, and from January 31 to March 7, 1986. The PVOUVS instrument operated on a cycle synchronized with the spacecraft spin period of ~13 sec. During each cycle the instrument collected data through its $1.4° \times 0.14°$ field of view as it scanned across the sky along a swath which varied from 20° to 80° in length. The data collected ideally represented the brightness of solar Lyman-α reasonantly scattered from atomic hydrogen in a swath of Comet Halley's coma 1.4° wide and 20° to 80° long. The resolution along the swath was determined by the integration time which varied from 8 to 32 msec or 0.19° to 0.75°. The data were collected for a period of 1 hr and the resulting 230–270 swaths were averaged together in order to improve signal-to-noise. A copy of this averaged data set, together with other ancillary information such as background, which consists of Lyman-α scattered by interplanetary hydrogen, was provided by A. I. F. Stewart.

3. MODELING ANALYSIS

The general approach adopted here is to simulate the spatial distribution of H atoms and Lyman-α resonance scattering in the coma of Halley and then compare this with the data described above. The simulation was accomplished with the MCPTM which is described in detail in the earlier papers by Combi and Smyth (1988a,b; hereafter referred to as Paper I and Paper II). For the parent molecule H_2O and its hydrogen-bearing daughter products H and OH, MCPTM employs a spherically symmetric fluid model in the inner collisional coma interfaced with a Monte Carlo particle treatment for the transitional and collisionless regions of flow in the outer coma. The fluid model provides the density, velocity, and temperature of the outflowing gas in the inner coma, which, in turn, are used by the Monte Carlo section of MCPTM to compute the velocity and spatial distribution of H in the outer coma. The distribution of H from H_2O and OH in the coma is determined by the photochemistry, elastic collisions, radiation force on H due to scattering of solar Lyman-α photons, the time-dependent production of H_2O, and loss of H due to charge exchange with solar wind protons, ionization by solar wind electrons, and photoionization. While all these processes are described in detail in Paper I, the updating of certain rates and the fact that we are interested in Comet Halley rather than Comet Kohoutek require some brief rediscussion of the photochemistry, model production rate, and g factor.

The kinetics of the photochemistry have changed slightly. The branching ratios for the various reactions are the same as in Paper II; however, the velocity distribution of the H and OH from H_2O dissociation has been altered in accordance with Crovisier (1989) who took into account the conversion of some of the dissociation energy into vibration and rotation. The result is roughly a 10% decrease in velocity of the fragments relative to that reported in Paper II. This modified photochemistry has also been used in all published MCPTM related work since Paper II. The composition of Halley's atmosphere is principally H_2O (~80%). Other H-bearing molecules H_2CO and HCOOH have been inferred to be present at levels <10%, leaving H_2O to generate >90% of the H. As a result, H_2O was assumed to be the only source of H.

In order to run the MCPTM, a production rate for H_2O is required. Since the H_2O production rate varies substantially over the several weeks needed to form the H coma, it is necessary to assume some time-dependent rate profile in the model. The rate profile shown in Fig. 1 reflects the long-term variation of H_2O production and was derived from a compilation of H_2O production rates based on various Halley observations between 2.5 AU preperihelion to 2.5 AU postperihelion given in Combi (1989). This range easily encompasses the time period of interest here between late December of 1985 and early March of 1986. With the exception of the model calculations shown by the solid line in Fig. 5 and by the triangles in Fig. 6, which will be discussed later, the production rate in Fig. 1 is employed in all model comae calculations. In principle one should iterate the production rate history by utilizing the new history derived from comparing the data to the model comae to recalculate the MCPTM comae. The newly recalculated comae should then be compared to the data to derive the next iteration

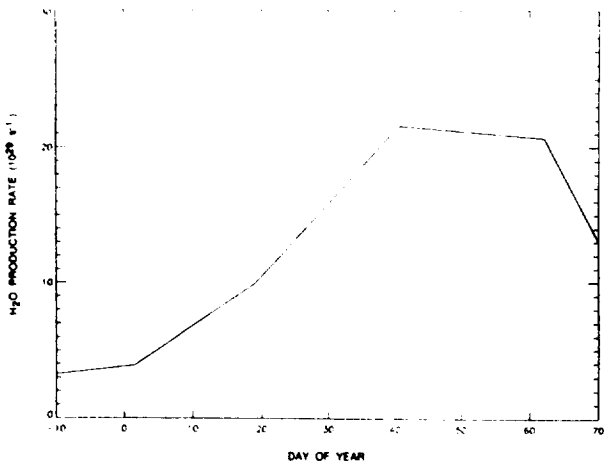

FIG. 1. Model production rate. H_2O production rate vs day of the year that is used in the MCPTM as derived from a variety of observations and given by Combi (1989).

of the history. This process should be repeated until convergence. In this study the iteration was terminated after the first iteration, since as shown in Fig. 2, the model and the data are already in close agreement.

The g factor used in the MCPTM to calculate the brightness of the coma and the radiation force on the H atoms was taken to be given by

$$g(t) = 1.73 \times 10^{-3} \frac{f(v)}{r^2(t)} \left(\frac{F(t)}{3.472 \times 10^{11}} \right)$$

photons atom^{-1} sec^{-1},

where $r(t)$ is the heliocentric distance in AU of the comet at time t, $F(t)$ is the Lyman-α solar flux in units of photons cm^{-2} sec^{-1} at the longitude appropriate to Comet Halley at time t, and $f(v)$ is the Lyman-α flux profile (Lemaire *et al.* 1978) expressed as a function of heliocen-

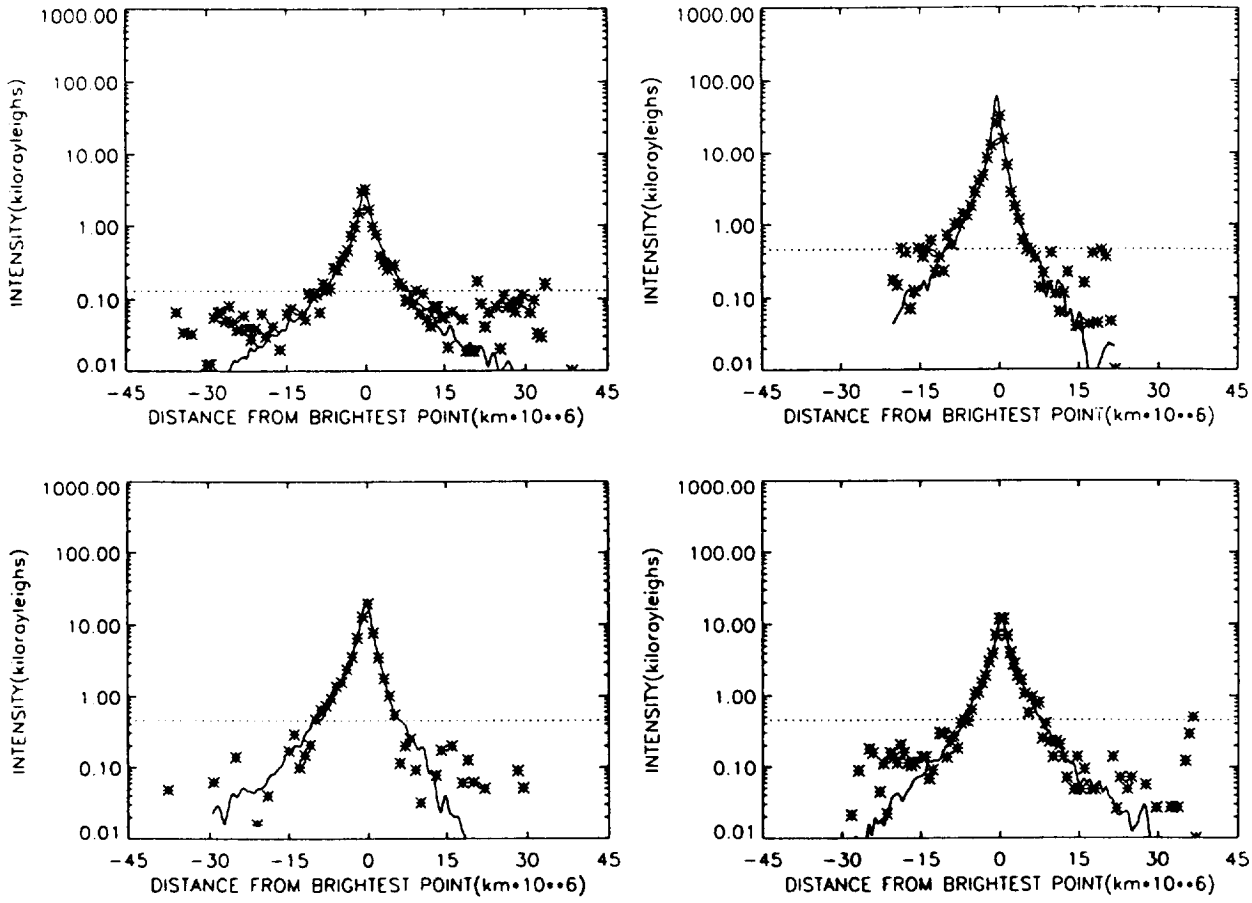

FIG. 2. Comparison of model and data. The brightness profiles in kilorayleighs are shown along the swath as a function of the distance from the brightest point. The observations (* symbols) and corresponding MCPTM (solid lines) with a plane-parallel correction for optical thickness are compared for four profiles. The various figures (top left, top right, bottom left, bottom right) represent Jan. 4 (day 4), Feb. 9 (day 40), Feb. 24 (day 55), and March 6 (day 65), respectively. The dashed lines show the background values, already subtracted from the data, for the Lyman-α scattered by the interplanetary hydrogen as provided by Stewart. These background values are typical of PVOUVS observations acquired on other days. It appears that there is still some additional background not included in the interplanetary hydrogen values. The Sun is to the right.

tric velocity and normalized so that its value at line center, i.e., the dimensionless quantity $f(v = 0)$, is unity. The normalization of the $1.73 \times 10^{-3} f(v)$ factor corresponds to a total flux of 3.472×10^{11} photons cm^{-2} sec^{-1}. The term $F(t)/3.472 \times 10^{11}$ effectively renormalizes $g(t)$ to the value of the Lyman-α flux present at the time of interest. $F(t)$ for the period between December 1985 and April 1986 was provided by Stewart (1991, private communication), who used the 1989 compilation of SME (Solar Mesosphere Explorer) Lyman-α flux measurements to compute the fluxes at Halley's longitude.

Recently, Combi and Feldman (1993) have argued that the SME Lyman-α brightnesses should be ~16% larger. They noted that observations by the SUSIM (Solar Ultraviolet Spectral Irradiance Monitor) experiment, which was designed explicitly to obtain accurate (better than 5%) absolute calibration and was flown in August 1985, indicated a solar Lyman-α flux that was 16% greater than the value on the same date in the current version of the SME data base. Furthermore, their comparisons of nearly simultaneous IUE observations of OH and H in Comet Halley, and similar but previously published results for Comet P/Giacobini–Zinner, are brought into nearly exact agreement when the larger solar Lyman-α fluxes are used. As a result, $1.16F(t)$ was actually employed in the calculations. Strictly speaking, one should employ the line center flux rather than the total Lyman-α flux in the formula for g. However, in the absence of measurements of the line center flux, using the total Lyman-α flux is probably the best that can be done. Moreover, the fact that the H atoms scatter Lyman-α photons anisotropically must also be taken into account. In the final calculation for the brightness of the H coma, the brightness output from the MCPTM was modified by multiplying by the following expression for the phase function of H atoms scattering Lyman-α photons, $P(t) = 0.942 + 0.25 \cos^2(\theta(t))$, where $\theta(t)$ is the Sun–comet–PVOUVS angle at the time, t, of observation.

The particle trajectories for this model were integrated for a period of time equal to 4×10^6 sec, spanning a time interval from the time of observation to 4×10^6 sec before. This is ample time for the hydrogen coma to fully develop. The number of particles employed in the simulation of a given swath was 20,000, which proved to be sufficient to provide favorable statistics where the data statistics were also favorable. The MCPTM grid was in each case a 6×10^5 km by 6×10^5 km square which for almost every measurement is smaller than the resolution along the swath.

MCPTM generates a two-dimensional brightness distribution of the solar Lyman-α flux scattered by the H coma in the skyplane of PVOUVS. As described above, the PVOUVS measures, however, a swath of brightness generated by a 1.4° × 0.14° slit scanning and integrating across the coma. Thus, the MCPTM output was convolved with the PVOUVS slit function applied along the trajectory of the data swath to produce an MCPTM simulation of the PVOUVS scan. The model brightness along the swath was then normalized to the data by overlaying and shifting vertically until some optimal level of overlap occurred. The H_2O production rate implied by the data was determined by the ratio of the normalized model profile to the unshifted model profile. Selected examples of this fitting procedure are shown in Fig. 2 and will be discussed later. This method of matching profiles appears to yield production rates which are reproducible to roughly 5%. Prior to matching the data, a background subtraction was performed. The Lyman-α background intensity which is primarily due to resonant scattering by the interplanetary hydrogen was provided by Stewart who used the Ajello (1990) model of Lyman-α scattered from this source.

In practice, the profile fitting procedure was controlled principally by the data roughly between 1.5×10^6 and 3×10^6 km. The brightest point and the points within 1.5×10^6 km of that point were ignored in the overlaying procedure because of the uncertainty in the pointing direction of PVOUVS. (There is an uncertainty of about 0.25° in the position of the brightest point, i.e., the brightest point is not recorded at its true position in the coma.) For the other data points which are farther away, the consequences of pointing error are relatively less important since the brightness gradients diminish with distance from the nucleus. Points beyond 3×10^6 km were also considered in the profile fitting procedure, but were allowed less weight because of the increasing importance of noise and uncertainty in the amount of Lyman-α background from the interplanetary hydrogen and because it was easier to decide the optimal overlap by including fewer points even when an excellent match was attainable.

Another potential problem with the analysis of the region near the brightest point is that the hydrogen coma displays a notable optical thickness to Lyman-α within roughly 1.5×10^6 km of the brightest point. The proper treatment of this multiple scattering problem is beyond the scope of MCPTM and at least in principle is nontrivial. As an attempt to contend with the multiple scattering, an extra correction to the brightness generated by MCPTM was optionally included. The correction was based on the radiative transfer calculation of McElroy and Yung (1975). Their approach is valid for a semi-infinite plane parallel scattering atmosphere observed at normal incidence which is not the same as the problem of scattering from the approximately spherical hydrogen coma of Halley observed at finite angles to the direction of insolation. Recently, however, a radiative transfer (RT) model, which was initially developed by Anderson

and Hord (1977), was applied to the hydrogen Lyman-α cometary coma by Combi and Feldman (1993). Although there are some significant assumptions in RT, such as a spherical coma and no bulk flow of H, near the nucleus where the optical depth is significant the RT cometary model is nevertheless quite accurate. The RT model was run for the conditions of February 24, 1986, and compared to the plane parallel corrected model used here. These results are discussed in Section 4.

This profile fitting procedure was utilized on only a small fraction of the many Lyman-α swaths. The data that were either contaminated, for example, by light from Venus, or that passed too far from the nucleus, were discarded. The remaining data were divided into sets according to the day that they were measured. From these, only the brightest and longest swaths were compared to the appropriate model runs. Table I contains H_2O production rates with one estimate per day for most of the days that PVOUVS observed the Lyman-α coma.

TABLE I
H_2O Production Rate for Comet Halley Determined from the Lyman-α Observations

Date		Heliocentric distance (AU)	H_2O production rate (10^{29} molecules sec^{-1})
1985	Dec. 28	1.06	2.37
	29	1.59	2.41
	30	1.56	3.11
	31	1.53	2.86
1986	Jan. 1	1.49	2.78
	2	1.46	3.53
	3	1.43	3.71
	4	1.39	4.0
	5	1.36	4.03
	6	1.32	3.88
	Feb. 1	1.10	11.3
	4	0.59	14.4
	8	0.59	14.9
	9	0.59	17.8
	10	0.59	17.9
	11	0.59	15.7
	12	0.59	15.7
	13	0.59	16.0
	14	0.60	18.0
	15	0.60	17.8
	16	0.61	17.1
	17	0.61	14.4
	18	0.62	12.5
	19	0.63	12.8
	20	0.63	14.2
	21	0.64	14.4
	22	0.65	14.3
	23	0.66	13.0
	24	0.67	14.0
	25	0.68	13.7
	26	0.69	13.6
	27	0.70	13.8
	28	0.71	13.7
	March 1	0.73	12.8
	2	0.74	11.2
	3	0.75	11.1
	4	0.76	9.49
	5	0.78	7.3
	6	0.79	8.01
	7	0.81	7.40

4. DISCUSSION AND CONCLUSION

Figure 2 compares MCPTM model brightnesses (solid line) and the PVOUVS data brightnesses (asterisks) described above. Plotted is the log of the intensity against distance along the swath from the brightest point (the Sun is to the right). The plots (top left, top right, bottom left, bottom right) correspond to January 4, February 9, February 24, and March 6, 1986 (day of year 4, 40, 55, and 65), respectively, and more or less span the time when PVOUVS was observing Halley's hydrogen coma. Examining the graphs it is clear that beyond about ±10 million km from the brightest point noise dominates the data and a comparison is not possible. The wiggles in the model at similar distances are the statistical fluctuations arising from the Monte Carlo nature of the simulation. At smaller distances, the model matches the data very well except possibly for the brightest point and/or its immediate neighborhood.

The case in point is Fig. 2 top right, which corresponds to February 9. Here the second brightest point is too far to the inside of the model curve. Since this same pattern persists on neighboring days, it is unlikely to be an artifact. A possible explanation is that the data reflect a change in the production rate that is not contained in the production rate function (Fig. 1) adopted in the MCPTM. As mentioned in the previous section, the MCPTM effectively employs a secular production rate which represents the long-term trend of H_2O emission from Halley. In reality the actual release of H_2O is known to be variable on time scales of days or less. Since Halley was particularly close to PVOUVS on February 9 (0.39 AU; on Jan. 4, Halley was 1.39 AU from PVOUVS for comparison), the slit was able to resolve smaller distances and thus was most sensitive to changes in the production rate on relatively short time scales. The other examples, particularly February 24, appear well matched by the model everywhere.

Figure 3 displays the brightness along a swath on February 24 for three different models. February 24 was chosen because the coma was relatively optically thick on that date. The dashed line represents the RT model run for a production rate of 1.6×10^{30} sec^{-1} and a temperature of 14,000 K for the hydrogen. Since the opacity depends on the velocity distribution of the hydrogen atoms,

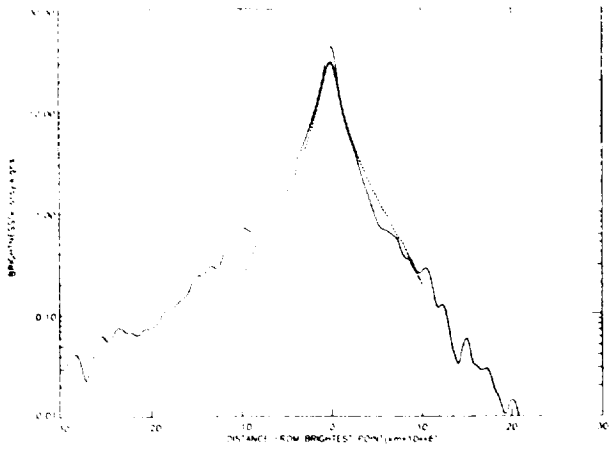

FIG. 3. Effect of optical depth. The brightness profiles in kilorayleighs are shown along the Feb. 24 swath as a function of the distance from the brightest point. The dotted line corresponds to the RT model while the lower solid line is the plane-parallel corrected MCPTM for optical depth, and the higher solid line is the MCPTM without any correction for optical depth. The Sun is to the right.

a temperature is required by the radiative transfer calculation to approximate the effect of the true velocity distribution. The temperature of 14,000 K was shown (Combi and Feldman 1992, 1993) to best represent the average H atom velocity distribution in the optically thick portion of the model. The sudden cutoff of the RT model beyond about 10 million km is simply due to reaching the end of the RT grid. The lower of the solid curves is the MCPTM model run for the same production rate and corrected using the results of McElroy and Yung (1975) with the same temperature. Clearly the corrected MCPTM and the RT model are quite similar in the region where the optical depth is significant. The shape of the profiles is the same, and the MCPTM is only slightly brighter (a few percent) than the RT model. Consequently, the corrected MCPTM is able to reasonably take into account the effect of multiple scattering by the hydrogen coma. It should not be assumed, however, that the corrected MCPTM replaces the RT model. The averaging effect resulting from the convolution with the PVOUVS slit is largely responsible for the agreement. The preconvolution two-dimensional model brightnesses are substantially less similar so that significant discrepancies would be expected to arise in sufficiently high-resolution observations of the optically thick region. Beyond the vicinity of the brightest point, the two models deviate due primarily to the fact that the RT model is a spherically symmetric model and the more realistic hydrogen distribution in the MCPTM is asymmetric because of radiation pressure effects. The higher solid line in Fig. 3 is the uncorrected MCPTM model which assumes an optically thin atmosphere. The optically thin MCPTM is about 20% brighter

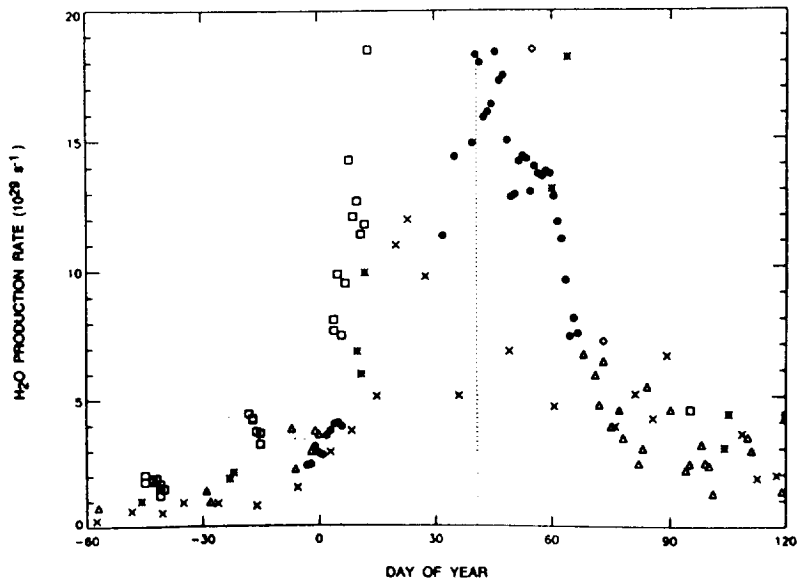

FIG. 4. H_2O production rates for Comet Halley. The production rates in units of 10^{29} molecules sec^{-1} are shown as a function of the day of the year from Nov. 1, 1985, to April 30, 1986, for a variety of measurements. The symbols refer to the following: (Δ) H_2O production rates determined from IUE data for OH emission by Combi *et al.* (1993), (□) H_2O production rates determined from the revised analysis (Smyth *et al.* 1993) of the 6300-Å emission data for atomic oxygen originally published by Magee-Sauer *et al.* (1990), (×) H_2O production rates determined from 18-cm OH radio observations by Bockelée-Morvan *et al.* (1990), (◇) H_2O production rates determined from rocket observations of H Lyman-α emission by McCoy *et al.* (1992), (*) H_2O production rates determined from 6300-Å emission observations of atomic oxygen by Fink and DiSanti (1990), (●) H_2O production rates determined in this paper from MCPTM analysis of H Lyman-α observations in Table I.

than the MCPTM corrected for optical depth near the center. The correction will be less for March and early January since the activity of the comet is lower, leading to a thinner H coma. It will also be smaller since the comet PVOUVS distance is greater and thus the spatial resolution is less. Larger corrections ~40% will occur for data taken near perihelion (Feb. 9) when the comet is highly active and the comet PVOUVS distance is smaller. In any case, the corrected MCPTM model appears to be able to generate the proper brightnesses.

In Fig. 4, the H_2O production rates in Table I are compared with those rates obtained by other observers. Perihelion for Comet Halley, which is on February 9 (day of year 40), is indicated by the dotted vertical line. The solid circles are for the H_2O production rates determined from the MCPTM analysis of the PVOUVS Lyman-α brightness measurements of Halley's hydrogen coma between late December 1985 and early March 1986. The other symbols represent H_2O production rates derived from other types of measurements for the period between early November 1985 and late April 1986. These do not exhaust all the measurements of Comet Halley's water production rates obtained in the relevant time interval, except possibly near perihelion. However, they are sufficient to illustrate how the new rates stand in reference to other determinations of the H_2O production rates.

As is clear from Fig. 4, toward late December 1985 and early January 1986, our production rates blend in well with the IUE OH measurements (Δ symbols) by Combi *et al.* (1993), who also used the MCPTM approach. In early January 1986 there appears to be a substantial discrepancy between the revised H_2O analysis (□ symbols) of (Smyth *et al.* 1993) of the 6300-Å emission data for atomic oxygen originally published by Magee-Sauer *et al.* (1990). However, the aperture employed by Magee-Sauer *et al.* was a 0.058° disk while the PVOUS aperture was a 1.4° × 0.14° slit. Consequently, the sharp increase in the production rate obtained by (Smyth *et al.* 1993) would be expected to appear in the much larger PVOUVS aperture somewhat after the last PVOUVS observation on January 6. Beyond January 6 there is a gap in the PVOUVS data lasting into January 31. Continuous acquisition of data resumed on February 1 (day of year 32). The MCPTM production rate rises above 1.1×10^{30} sec^{-1}, until near March 1 (day of year 60), after which it falls and joins smoothly with the IUE-derived production rates of March 9 (day of year 68) and beyond.

For the period between February 7 and March 7 (day of year 38 to 66), there are a few H_2O production rate determinations from the rocket observations (◇ symbols) of Lyman-α of McCoy *et al.* (1992) and the O (^1D) ground-based observations (* symbols) of Fink and DiSanti (1990). Within their estimated errors of about 50%, these determinations are quite consistent with the MCPTM results. Finally, there is also an extensive set of 18-cm OH radio observations (× symbols) for this time interval recently converted to H_2O production rates by Bockelée-Morvan *et al.* (1990). These are in poor agreement with the MCPTM results during this time. The interpretation of OH radio data, however, is complicated by a number of difficulties with the most insidious being the quenching of OH excited states. This is most severe at high production rates. Indeed, Fig. 4 shows that the agreement between MCPTM and the radio derived rates is only poor very near perihelion where the highest production rates occur.

The production rates calculated from the OH radio data shown in Fig. 4 have a quenching correction included. Yet whenever the production rate is large, they still systematically tend to undercut the production rates derived from the other types of observations by a factor of about three. The calculation of quenching is based upon a scaling relation for the value of the quenching radius which is a function of the production rate of H_2O (Schloerb 1988). It is assumed in the derivation of the scaling relation that the ratio of ions/neutrals, plasma velocity, and plasma temperature (velocity distribution) at the quenching radius do not depend on the production rate and more importantly, the quenching radius itself. This is quite probably incorrect, and an effective means of reducing OH 18-cm radio brightnesses to production rates must await a proper description of the cometary plasma for different production rates and heliocentric distances.

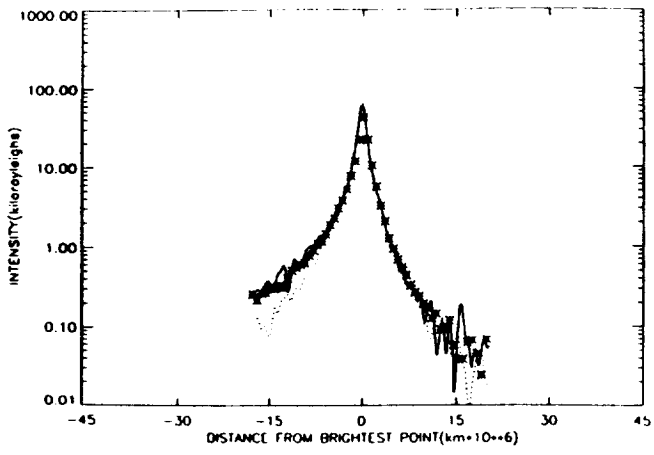

FIG. 5. Comparison of model to Feb. 8 data. The brightness profiles in kilorayleighs are shown along a Feb. 8 swath as a function of distance from brightest point. The observations are indicated by the * symbols. The MCPTM with a plane-parallel correction for optical thickness and for the production rate in Fig. 1 is indicated by the dotted line. The MCPTM with a production rate which is increased to 3.5×10^{30} molecules sec^{-1} between January 10 and January 30 is indicated by the solid line. The Sun is to the right.

If the factor of three correction is applied to the OH radio data around January 22, the result is that the sharp increase that the O(¹D) shows around January 10 to a value of almost 2×10^{30} sec^{-1} on January 13 may actually continue to over 3×10^{30} sec^{-1} by about January 22 and then fall to the PVOUVS rate on February 1 of 1.1×10^{30} sec^{-1}. Then Halley's activity would actually peak about 2½ weeks before perihelion, which contrasts with the usual expectation of maximum water emission when closest to the Sun. It must be emphasized, however, that any such extrapolation of the OH radio data should be regarded as speculative until proper means of interpreting the OH result are developed. There is, however, independent evidence in the PVOUVS measurements themselves that the factor of 3 may be correct.

Since the coma requires several weeks to develop due to its large spatial extent, the PVOUVS profiles must reflect the production rate history of the comet for a similar period of time. Thus, the PVOUVS data nearest to the gap may be studied for evidence of the great increase in comet activity. Unfortunately, the data in this period seem to be rather noisy (see Fig. 2, top right) and also span a relatively small spatial scale. An exception at least with respect to the amount of noise is an observation taken on February 8 and shown in Fig. 5. The dotted line is the model with the usual underlying production rate (Fig. 1) which clearly underestimates the antisunward data beyond 10^7 km. The solid line has a production rate which is similar to that shown in Fig. 1 except that between January 10 and January 30 a large production rate of 3.5×10^{30} sec^{-1} is assumed. Clearly, the match is significantly improved. Some caution must be exercised in interpreting Fig. 5. Although the background provided with the data was subtracted, it is apparent from Fig. 2 that there still may be some additional background which is not taken into account. Therefore, it is likely that the data for February 8 in Fig. 5 are also somewhat high. As a result, the production rate of 3.5×10^{30} sec^{-1} used in the model should be regarded as an upper bound. In order to obtain an excellent match between the MCPTM with the usual production rate and the data on the antisunward side, an extra background subtraction of 0.2 kR must be performed. Such a large additional correction (~50% of the initial background removed) results in an unsatisfactory fit on the sunward side, however, so that the background cannot be adjusted to explain the increased tailward abundance in the coma. The presence of an elevated preperihelion production rate in the February 8 profile is also supported by a preliminary reanalysis of the H Lyman-α image acquired by PVOUVS from February 2 to February 6, 1986, which was analyzed earlier by Smyth *et al.* (1991) for the production rate in Fig. 1. If an additional H_2O (triangular shaped) source with a time duration of ±6 days about a maximum production rate of 3.6×10^{30} sec^{-1} on January 23 is assumed, the newly computed Lyman-α contours provide a better fit to the observations, particularly in the tail portion of the coma, than the contours based on the H_2O production rate in Fig. 1. The presence of an elevated preperihelion production rate is therefore supported by the PVOUVS observation.

Figure 6 is a comparison between Stewart's (1987) H_2O

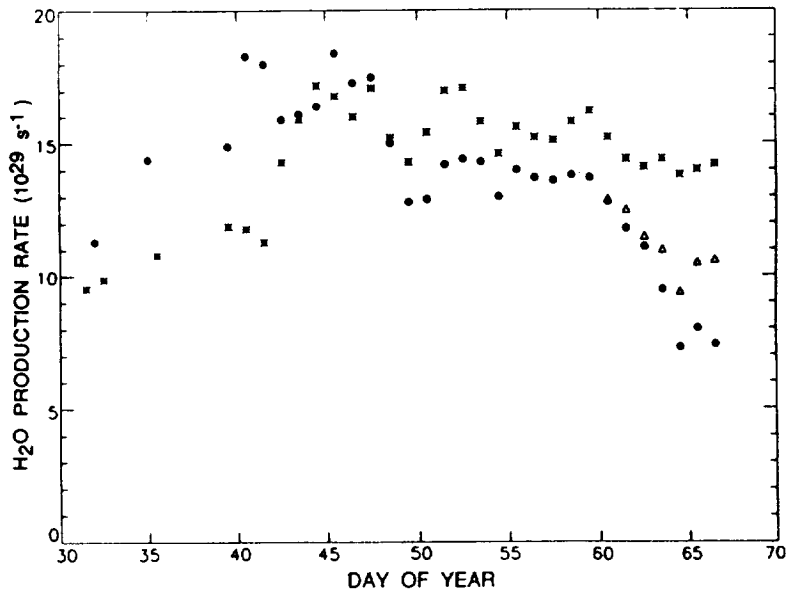

FIG. 6. Comparison of H_2O production rates for the MCPTM and Stewart. The solid dots represent the MCPTM Lyman-α results in Table I, and the asterisks are the earlier values of Stewart (1987). The MCPTM Lyman-α results for the production rate in Fig. 1 held constant after day of year 55 are shown by the Δ symbols.

production rates (asterisks) and those of the MCPTM (solid dots) which includes a correction for optical thickness. The MCPTM and Stewart results are fairly similar between about February 14 and March 1 (day of year 45 and 60). In both cases, there is, on the average, a high production rate after perihelion which tends to diminish somewhat after February 19 (day of year 50). Both models display oscillatory behavior. The MCPTM oscillations seem to be somewhat more subdued but seem to follow those of Stewart. The greatest differences lie at early and late times when the MCPTM is significantly higher and lower than Stewart, respectively.

A comparison between the results in Fig. 6 is not straightforward because of the considerable differences not only in the models employed to convert data brightnesses to production rates, but also in the manner of utilization of data for the derivation of production rates. The MCPTM attempts to treat the hydrogen realistically, accounting for both the dynamics and chemistry of the H atoms in a proper fashion as previously described. The Stewart model is a one-velocity (11.3 km sec^{-1}, the harmonic mean of the 8 and 18 km sec^{-1} principal velocity components of hydrogen from photodissociation, Stewart 1993, private communication) Haser model. The corrected MCPTM also accounts for optical depth effects, the H scattering phase function, and the more recent SME (1989) solar Ly α fluxes plus a 16% further enhancement which results in a g factor nominally 10–20% higher than in Stewart. The treatment of the data is also dissimilar in important ways. Stewart (1987) averages the data along the swath within $\pm 1.15°$ of the brightest point. In addition, Stewart also combines the above averages from all the swaths which intercept the comet nucleus on a particular day. On the other hand in this study, while the individual swaths were considered, the brightest point and a neighborhood of about ± 1.5 million km were ignored to minimize any potential errors introduced by the treatment of optical depth effects and the pointing uncertainties discussed earlier.

For observations at early times (i.e., between January 30 and February 14, before day of year 45), the lower rates inferred by Stewart (1987) are the result of examining the region near the brightest point where the substantial optical depth shields some H from view. At later observational times, the higher rates deduced by Stewart may be a consequence of the swath averaging described above which corresponds to an area about the comet increasing to 5 million km × 8 million km by March 7 (day of year 66). This large area contains substantial contributions of material produced by the nucleus at times before the day of interest when the production rate was relatively flat and hence may conceal the sharp decline suggested by the IUE observations (Fig. 4) which begins toward the end of the PVOUVS observation period. In this study, the production rate determination is controlled by points of a single swath at a few million kilometers from the intensity peak and may in March reflect more recently emitted material. Furthermore, the phase function is >1 and also decreases the inferred production rate. It could, however, be reasonably pointed out that the sharp drop in the underlying production rate curve (Fig. 1) may be responsible for the rapid decrease in the production rates beyond March 1 (day of year 60). In order to test this hypothesis, simulations were done with a production rate profile similar to that of Fig. 1 except that beyond February 24 (day of year 55) the production rate was held constant. The triangles in Fig. 6 are the result. Clearly a fall in H_2O production is still evident which indicates that the merging into the IUE observations is not an artifact of the choice of the underlying production rate curve used in the MCPTM.

In conclusion, the simulation of PVOUVS measurements of Lyman-α scattered from the Halley coma is another example of the successful application of the MCPTM to cometary comae. The spatial brightness distribution is very well reproduced as long as the underlying production rate is sufficiently representative of the actual activity of the nucleus. The production rates derived here are consistent with most of those from other types of measurements which overlap the PVOUVS data acquisition period. They also blend with the early March IUE results, in contrast to the earlier results of Stewart (1987). Moreover, if it is reasonable to suppose that an improved calculation of the quenching radius could alter the 18-cm OH radio results by a factor of ~2 to 3, then there is currently no reason to expect a fundamental discordance with any other observations.

The MCPTM rates, considering the substantial differences in the modeling, corroborate Stewart (1987) rates between about February 10 and March 1, including the 7-day oscillation. In early February and in March the differences may be respectively reconciled by optical depth effects and differences in the spatial scale of the data-derived quantities which are compared to theory. Finally, the spatially detailed analysis of February 8 PVOUVS data suggests an extended period of high water production, possibly to almost twice the perihelion values, for much of the time between January 10 and January 30 when PVOUVS was not observing. This is consistent with the rapid rise seen in $O(^1D)$ data (Fig. 4) starting around January 10, the $O(^1D)$ deduced water production rates of 2.90×10^{30} and 2.68×10^{30} sec^{-1} on January 16 and January 17 respectively of Smyth *et al.* (1995), and production rates of over 3×10^{30} sec^{-1} near January 22 if the OH radio derived H_2O production rates are low by a factor of ~3.

ACKNOWLEDGMENTS

We are grateful to A. I. F. Stewart for helpful discussions and for providing the Lyman-α scan data for the coma of Comet Halley obtained from the ultraviolet spectrometer aboard the Pioneer Venus Orbiter spacecraft. This research was supported by the NASA Planetary Atmospheres Program under Contracts NASW-4329 and NASW-4496 to Atmospheric and Environmental Research, Inc., and under Grant NASW-3417 to the University of Michigan.

REFERENCES

Ajello, T. M. 1990. Solar Lyman α sky background observations from Pioneer Venus Orbiter Ultraviolet Spectrometer: Solar wind latitude variation. *J. Geophys. Res.* **95.A9,** 14855–14861.

Anderson, D. E. Jr., and C. W. Hord 1977. Multidimensional radiative transfer: applications to planetary coronae. *Planet. Space. Sci.* **25,** 563–571.

Bockelée-Morvan D., J. Crovisier, and E. Gérard 1990. Retrieving the coma gas expansion velocity in P/Halley, Wilson (1987 VII) and several other comets from 18-cm OH line shapes. *Astron. Astrophys.* **238,** 382–400.

Combi, M. R. 1989. The outflow speed of the coma of Halley's comet. *Icarus* **81,** 41–50.

Combi, M. R., B. J. Bos, and W. H. Smyth 1993. The OH distribution in cometary atmospheres: A collisional Monte Carlo model for heavy species. *Astrophys. J.* **408,** 668–677.

Combi, M. R., and P. D. Feldman 1992. IUE observations of HI Lyman-α in Comet P/Giacobini–Zinner. *Icarus* **97,** 260–268.

Combi, M. R., and P. D. Feldman 1993. Water production rates in Comet P/Halley from IUE observations of HI Lyman-α. *Icarus* **105,** 557–567.

Combi, M. R., and W. H. Smyth 1988a. Monte Carlo particle trajectory models for neutral cometary gases. I. Models and equations. *Astrophys. J.* **327,** 1026–1043.

Combi, M. R., and W. H. Smyth 1988b. Monte Carlo particle trajectory models for neutral cometary gases. II. The spatial morphology of the Lyman-α coma. *Astrophys. J.* **327,** 1044–1059.

Crovisier, J. 1989. The photodissociation of water in cometary atmospheres. *Astron. Astrophys.* **213,** 459–464.

Fink, U., and M. A. DiSanti 1990. The production rate and spatial distribution of H_2O for Comet P/Halley. *Astrophys. J.* **364,** 687–698.

Lemaire, P., J. Charra, A. Jouchoux, A. Vidal-Madjar, G. E. Artzner, J. C. Vial. R. M. Bonnet, and A. Skumanich 1978. Calibrated full disk solar HI Lyman-α and Lyman-β profiles. *Astrophys. J.* **223,** L55–L58.

Magee-Sauer, K., R. Scherb, F. L. Roesler, and J. Harlander 1990. Comet Halley O(^{1}D) and H_2O production rates. *Icarus* **84,** 154–165.

McCoy, R. P., R. R. Meier, H. U. Keller, and G. R. Carruthers 1992. The hydrogen coma of Comet P/Halley observed in Lyman-α using sounding rockets. *Astron. Astrophys.* **258,** 555–565.

McElroy, M. B., and Y. L. Yung 1975. The atmosphere and ionosphere of Io. *Astrophys. J.* **196,** 227–250.

Schloerb, F. P. 1988. Collisional quenching of cometary emission in the 18 centimeter OH transitions. *Astrophys. J.* **332,** 524–530.

Smyth, W. H., M. R. Combi, and A. I. F. Stewart 1991. Analysis of the Pioneer Venus Lyman-α image of the hydrogen coma of Comet P/Halley. *Science* **253,** 1008–1010.

Smyth, W. H., M. L. Marconi, F. Scherb and R. L. Roesler 1993. Analysis of hydrogen Hα observations of the coma of Comet P/Halley. *Astrophys. J.* **413,** 756–763.

Smyth, W. H., M. R. Combi, F. L. Roesler, and F. Scherb 1995. Observations and analysis of O(^{1}D) and NH_2 line profiles for the coma of Comet Halley. *Astrophys. J.*, **440,** in press.

Stewart, A. I. F. 1987. Pioneer Venus measurements of H, O, and C production in Comet P/Halley near perihelion. *Astron. Astrophys.* **187,** 369–374.